Universität Stuttgart
ITSM
Institut für
Thermische Strömungsmaschinen
und Maschinenlaboratorium
Leiter:
Prof. Tekn. Dr. Damian Vogt

STUDY ON A RADIAL TURBINE STAGE WITH INLET GUIDE VANES FOR AN ORC PROCESS WITH AN ELECTRICAL OUTPUT OF 3,5 kW

Studienarbeit

vorgelegt von

Eduardo López

Matr.-Nr.: 2768971

2013

Betreuer: Dipl.-Ing. Mirko Ilievski

Acknowledgements

I could not have performed this thesis without the support of my family. Thank you.

To my friends who supported me more than they think.

To all my ERASMUS friends who helped me and made from this experience an important part of my life.

I want to thank the ITSM and my supervisor, Mirko Ilievski, who helped me a lot.

Abstract

The goal of the present thesis is initially to determine if the ideal gas model is valid for the modelling of the refrigerant R-245fa for an ORC expansion in a radial turbine. Therefore, the expansion will be calculated using an ideal gas model and a real gas one. The results from both calculations will be compared in order to determine if the ideal gas model leads to valid results. After deciding which of the models leads to better results, this model will be used to perform an optimization of the radial turbine by varying its inlet width and the rotational speed.

Contents

List of Figures

List of Tables

Guide

This guide will help the reader to understand the structure of the report. It seeks to provide an easy way to find the information needed. The guide will present where to find the thoughts and ideas of the author.

What the reader will find on the following chapters is:

- Chapter 1: Introduction

The keywords of the project are: Organic Rankine Cycle, R-245fa and radial turbine. Chapter 1 has the objective of explaining these different concepts. The importance of this chapter stands on familiarizing the reader with these concepts.

- Chapter 2: Real/Ideal Gas assumption effects (1D)

Initially this chapter explains the different variables that are necessary to understand the differences between a real gas and an ideal gas. These are needed to calculate both models in with the used CFD solver. The parameters are then evaluated for the field of the expansion so that they can be used in the simulations. To conclude, the chapter presents a one dimensional design of the simulations drawing the possible effects of choosing the ideal gas model or the real gas one.

- Chapter 3: Real/Ideal Gas assumption effects

Firstly in this chapter, the setting on of the simulations is explained. The results of the ideal gas calculation and the real gas calculation are presented, discussed and compared to the expectations from the one dimensional design of Chapter 2.

- Chapter 4: Study on turbines with different inlet width for an ORC process with an electrical work output of 3.5 kW

In this chapter, turbines with three different widths are calculated in order to study the effects of inlet width on the turbine features. After considering the results of these first calculations, a second set of calculations is executed in order to optimize the turbines by changing their rotational speed. For all these simulations, the gas model utilized is the real gas model investigated in chapters 2 and 3.

- Chapter 5: Conclusions

The conclusions of the project are put together in this chapter. After a review of the targets accomplished by the project, a recommendation is given for further work on the topics threated.

Chapter 1: Introduction

In this chapter the foundations of the thesis will be explained. First, Organic Rankine Cycles will be analysed. Afterwards, the reasons for the election of refrigerant R-245fa for such processes will be described. Having understood what Organic Rankine cycles are, radial inflow turbines will be presented.

1.1. The Organic Rankine Cycle (ORC)

The Organic Rankine Cycle is a technology for electrical energy production from sources with a medium/low temperature level (< 250°C). It can use heat from processes such as solar thermal power, which would be otherwise wasted. Other applications from which an ORC recovers heat are: Solar energy systems or geothermal energy systems as read in [2].

The ORC is based on the Rankine Cycle. An ORC, though, uses an organic (containing carbon) compound as working fluid instead of water steam. These fluids used to have an elevate molecular weight. The boiling point of the organic fluids used in the ORC takes place at a lower temperature than the water steam phase change in a Rankine Cycle. The boiling temperature of the organic fluids working under ORC conditions usually are below 100 ℃. It makes possible to recover heat from a lot of different applications and produce additional power.

The ORC takes heat from a thermal cycle using a heat exchanger. The heat is used by the organic fluid to activate the turbine and produce electricity by using a generator to convert the mechanical power of the shaft of the turbine into electrical energy.

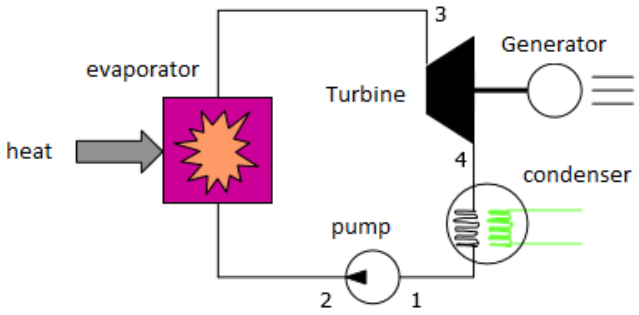

Figure 1.1: Organic Rankine Cycle parts

The ORC consists of four processes, which are illustrated in Figure 1.1:

- 1-2. Compression of the organic fluid in the pump.
- 2-3. Isobaric heating of the organic fluid in the evaporator.
- 3-4. Expansion of the organic fluid in the turbine.
- 4-1. Isobaric cooling of the organic fluid in the condenser.

A good way to understand the state of the working fluid through the process is to look at the p-h diagram in Figure 1.2. It shows the ORC on the p-h diagram of the working fluid, which for this application was R-245fa. The pump uses the refrigerant as liquid. The evaporator vaporizes the fluid from a liquid state to a saturated vapour state. The turbine expands the refrigerant being in vapour state. It is important that the turbine works with absence of humidity. The condenser then brings the vapour exiting the turbine to a saturated liquid state and the cycle is closed.

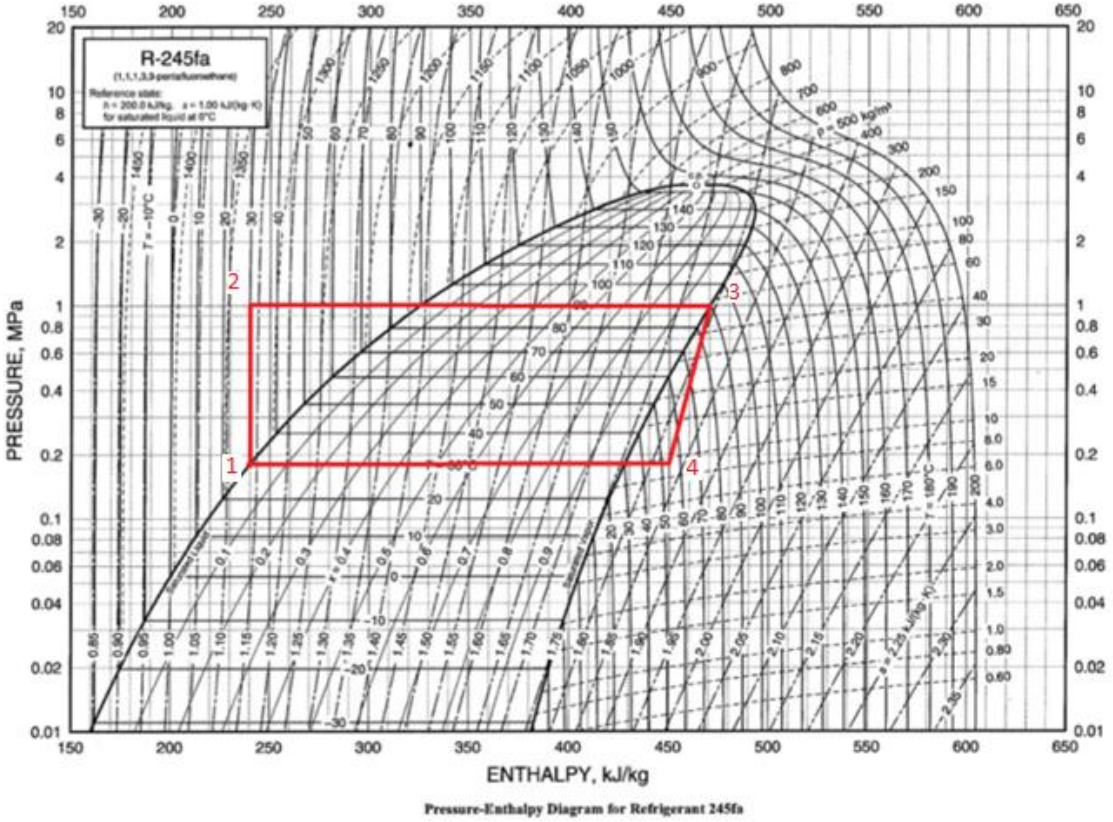

Figure 1.2: Organic Rankine cycle recovering heat from a CPV/thermal system from [1]

1.2. R-245fa

The cycle efficiency depends directly on the working fluid election. From the optimum working fluid study of [3], it can be concluded that important factors when selecting a working fluid are: toxicity, flammability, cost, thermal efficiency or compatibility.

Principal characteristics for the working fluid regarding studies [4, 5] are:

- Low environmental impact and high safety: The main parameters to be taken into account are the Ozone Depletion Potential, the GWP (Global Warming Potential), the toxicity and the flammability.
- High stability temperature. Organic fluids decompound and are deteriorated at high temperatures.
- Thermodynamic Properties
- Dry refrigerant: Saturated vapour curve with positive slope in the T-s diagram. No reheating is than required in order to avoid liquid formation in the turbine.
- High vapour density: Especially for fluid with low condensation properties.
- Commercial viability and moderate cost

The correct election of the working fluids also has to be based on a thermodynamic more detailed study. According to [6] and [7], a resume of the appropriate thermodynamic properties are the next:

- High density (ρ) in order to increase the mass flow and so reduce the size of the elements.
- High enthalpy of evaporation (ΔH_v): The enthalpy of evaporation is the energy required to transform a given quantity of a substance from a liquid into a gas at a given pressure. Being high, it allows greater heat exchange to be carried out in the phase change and avoid overheating or reheating.
- Low viscosity (μ) to increase heat transfer coefficient implying a low power consumption.
- High thermal conductivity (λ) to reach high heat transfer coefficients in the heat exchangers.

According to [8], as chain length and molecular weight increase, the molar heat capacity and entropy increase. Comparing, for example, R-11, R-123 and R-245fa, the longer molecular chain length of R-245fa means that the vibrational component of heat capacity will increase as well as entropy because of the greater movement of the molecule contributed by the length of the chain. The way in which entropy and enthalpy, affected by increased heat capacity, lead to an improved efficiency can be seen in Figure 1.3.

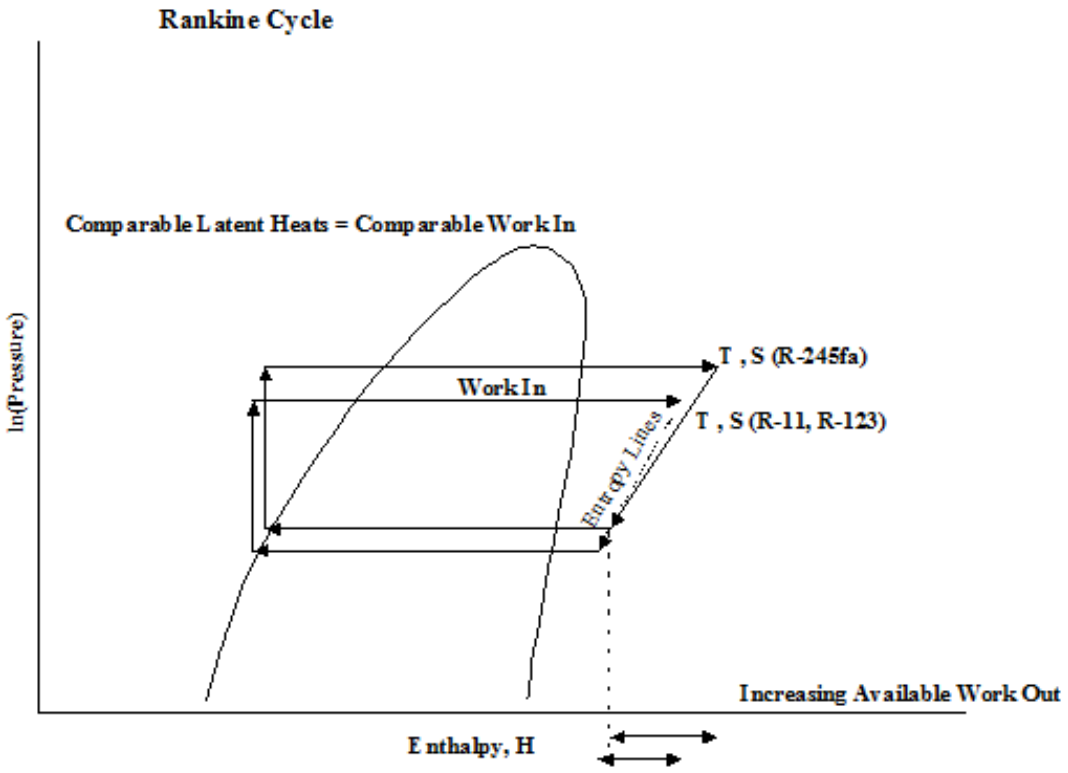

Figure 1.3: p-h diagram: Influence of Heat Capacity on Efficiency [10]

Figure 1.3 compares the cycle for R-245fa with two other refrigerants used for the same application. It shows how increased heat capacity leads to a higher output work.

From the NIST software [9], the properties of R-245fa are shown in Figure 1.4.

Properties of HFC-245fa	
Chemical Name	1,1,1,3,3-pentafluoropropane
Molecular Formula	CF3CH2CHF2
Molecular Weight	134
Flammability Limits in Air @ 1atm** (vol.%)	None
Flash Point *	None
Water Solubility in HFC-245fa	1600 ppm
ASHRAE Safety Group Classification	B1

*Flashpoint by ASTM D 3828-87; ASTM D1310-86
**Flame Limits measured at ambient temperature and pressure using ASTM E681-85 with electrically heated match ignition, spark ignition and fused wire ignition; ambient air.

Standard International Units*		English Units*	
Boiling Point °C @1.01 bar	15.3	Boiling Point (°F) @1atm	59.5
Freezing Point °C @1.01 bar	<-107	Freezing Point (°F)	<-160
Critical Temperature** (°C)	154.05	Critical Temperature** (°F)	309.29
Critical Pressure** (bar)	36.4	Critical Pressure** (psia)	527.9
Critical Density** (m3/kg)	517	Critical Density** (lb/ft3)	32.28
Vapor Density @ Boiling Point (lb/ft3)	5.921	Vapor Density @ Boiling Point (lb/ft3)	0.3697
Liquid Density (kg/m3)	1339	Liquid Density (lb/ft3)	83.58
Liquid Heat Capacity (kJ/kg K)	1.36	Liquid Heat Capacity (Btu/lb °F)	0.33
Vapor Heat Capacity @constant pressure, 1.01 bar (kJ/kg K)	0.8931	Vapor Heat Capacity @constant pressure, 1atm (Btu/lb °F)	0.218
Heat of Vaporization at Boiling Point (kJ/kg)	196.7	Heat of Vaporization at Boiling Point (Btu/lb)	84.62
Liquid Thermal Conductivity (W/m K)	0.081	Liquid Thermal Conductivity (Btu/hr ft °F)	0.0468
Vapor Thermal Conductivity (W/m K)	0.0125	Vapor Thermal Conductivity (Btu/hr ft °F)	0.0072
Liquid Viscosity (mPa s)	402.7	Liquid Viscosity (lb/ft hr)	0.9744
Vapor Viscosity (mPa s)	10.3	Vapor Viscosity (lb/ft hr)	0.025

*Properties at 77 °F / 25 °C unless noted otherwise
**NIST Refprop v 7.0

Figure 1.4: NIST properties of R-245 fa

As it can be seen in Figure 1.4, R-245fa shows a high critical temperature (154 °C), which means a higher efficiency of the refrigerating cycle with compared to the one of R-134a (101°C). Other advantages, as commented, for this refrigerant are its low viscosity, and high density.
Also important is accepting R-245fa as working fluid, namely the environmental characteristics in Figure 1.5.

Table 2 - Regulatory and Environmental Information

CAS Number	460-73-1
Ozone Depletion Potential	0
Global Warming Potential (100-yr time horizon)	950
US VOC status	Exempt
Exposure guidelines	
ACGIH TLV	None
OSHA PEL	None
WEEL (AIHA) TWA - 8 hrs (1)	300ppm
US DOT Hazard Class	Not regulated
US RCRA	Unused Material Not RCRA Waste
US TSCA Inventory Status	Listed
US SNAP Approval	Approved for use in new Centrifugal Chillers

Figure 1.5: Environmental characteristics and regulatory information of R.245fa from [8]

The most important values of Figure 1.5 that can be taken into account are the Ozone Depletion Potential, which is zero because it has no chlorine; And a GWP of 950 considering a 100 year time horizon, which in front of R-134a (1430) has a low value.

The thermodynamic and environmental properties of R-245fa make it the best refrigerant to use for low temperature heat recovery. The efficiency of the thermodynamic cycle will be, as explained, higher than with other refrigerants such as R-11, R-123. It has a higher critical temperature than R-134a, which allows more applications, is not flammable, and has better environmental properties than any other refrigerant, which is a factor that gains more importance every day.

1.3. Radial-inflow turbines

1.3.1. Description of the geometry and the flow

Radial-inflow turbines are appropriate for aircraft applications, space power systems and other fields where compact power sources are required. The principal advantages of radial-inflow turbines are high efficiency, ease of manufacture, sturdy construction and reliability.

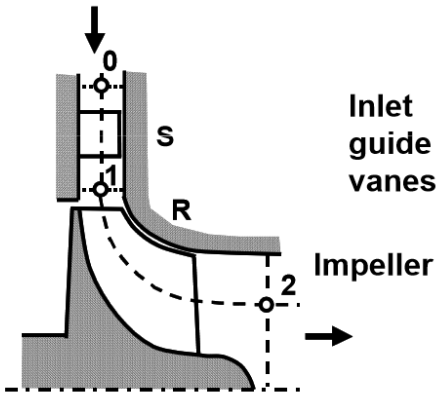

Figure 1.6: Reference plan notation taken from [9]

As can be observed in Figure 1.6, the flow enters the stator radially and leaves the rotor axially. Between reference planes 0 and 1 there is the stator. The rotor can be found between the reference planes 1 and 2. The radial turbine stage is defined between planes 0 and 2. The flow is not principally in the axial direction. Therefore the meridional direction will be the one taken into account. This is the mean direction of the streamlines projected into a plane containing the axis of the machine. It can be observed in Figure 1.7. Angles of the gas and of the blade will be measured relative to meridional direction.

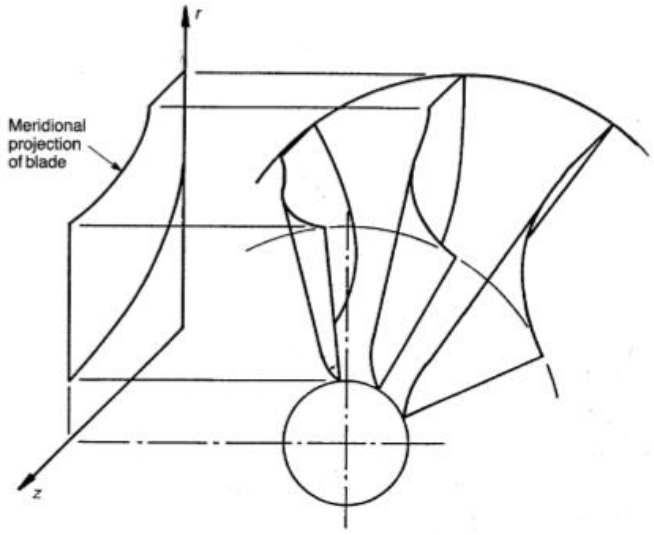

Figure 1.7: Meridional plane of an In-flow radial turbine from [10]

1.3.2. Velocity triangles

The velocity triangles, shown in Figure 1.8, are the basis of a one dimensional (1-D) design.

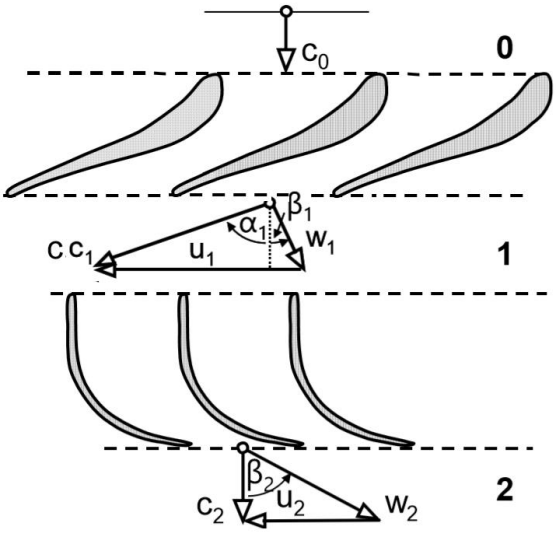

Figure 1.8: Velocity triangles from [11]

The velocities c are the absolute velocities of the fluid. The velocities u characterize the rotational speed of the blade. The blade is the reference for which the relative velocities W are interpreted. The horizontal projection of c_i is called c_{ui}. The vertical component of c_i is named c_{mi} because it is projected on the meridional direction. At the rotor exit, the blades are curved to turn the flow, so that the exit absolute velocity has little or no whirl.

In this work, the inlet impeller angle α_1 will be set close to 70°. Another consideration for the triangles will be $c_{u1} = 0.85u_1$. The explanation for this assumption, which is an optimum configuration for rotor inlet, can be found in [11] and is only a function of the number of blades, which is 12.

1.3.3. h-s diagram and isentropic efficiency

The flow of compressible fluid through a radial-inflow turbine involves large accelerations and decelerations, which may not be accomplished by external work transfers depending on whether they take place in a stationary duct or a moving row of blades. The concept of stagnation or total state, defined as that which the fluid would attain if it were brought isentropically to rest, is one of the basic fundaments to compressible gas dynamics. It follows from the definition of a stagnation state that the stagnation enthalpy is equal to the sum of the static enthalpy and the kinetic energy. Using specific values (per unit mass flow):

$$h_{ti} = h_i + \frac{1}{2}C_i^2 \tag{1-1}$$

Turbines are designed to convert the available enthalpy in a flowing fluid into useful mechanical work delivered at its output shaft. Mechanical losses occur between the rotor and the output shaft coupling as a result of the work done against friction in the bearings, glands, etc. For small machines, like the one studied in this work, it may amount to 5% or more. A detailed consideration of the mechanical losses in the turbine is beyond the scope of this thesis, since the shaft will not be studied.

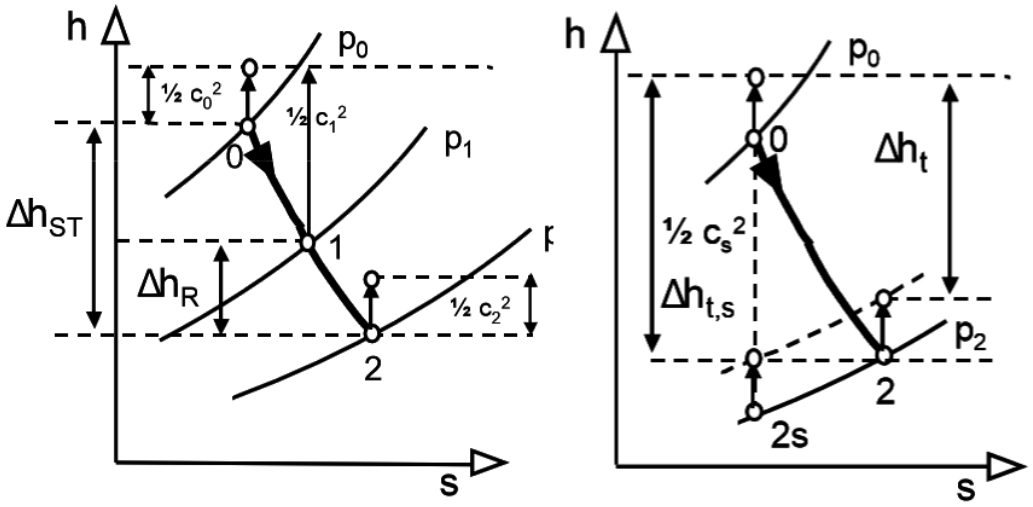

Figure 1.9: Mollier diagram of the process from [11]

Figure 1.9 shows a Mollier diagram representing the expansion process through an adiabatic turbine. The line 0-2 represents the actual expansion while line 0-2s describes the ideal or reversible expansion.

The actual turbine specific work is given by equation (1-2).

$$\Delta W_x = \frac{\dot{W}_x}{\dot{m}} = h_{t0} - h_{t2} = (h_0 - h_2) + \frac{1}{2}(c_0 - c_2) \tag{1-2}$$

It is called the steady flow energy equation. The ideal turbine rotor specific work is:

$$\Delta W_{max} = \frac{\dot{W}_{xmax}}{\dot{m}} = h_{t0} - h_{t2s} = (h_0 - h_{2s}) + \frac{1}{2}(c_1^2 - c_{2s}^2) \tag{1-3}$$

The different ways of interpreting efficiency depend on the usage of the exit kinetic energy. If it is not wasted, the efficiency taken into account is the total-to-total efficiency, presented in equation (1-4).

$$\eta_{tt} = \frac{\Delta W_x}{\Delta W_{max}} = \frac{h_{t0} - h_{t2}}{h_{t0} - h_{t2s}} \tag{1-4}$$

If the difference between the inlet and outlet kinetic energies is small and/or the values are very low, like in the expansion, (1-4) changes to (1-5).

$$\eta_{tt} = \frac{h_0 - h_2}{h_0 - h_{2s}} \tag{1-5}$$

If the exhaust kinetic energy is not useful and is wasted, the relevant adiabatic efficiency is the total-to-static one, showed in equation (1-6).

$$\eta_{ts} = \frac{h_{t0} - h_{t2}}{h_{t0} - h_{2s}} \tag{1-6}$$

If the velocities at inlet and outlet are negligible, static enthalpy can be considered as:

$$\eta_{ts} = \frac{h_0 - h_2}{h_0 - h_{2s}} \tag{1-7}$$

1.3.4. The continuity equation

Equation (1-8), is based on the fact, that in steady flows the mass flow rates of fluid entering and leaving a control volume are identical.

$$\dot{m} = \rho_i C_i A_i \tag{1-8}$$

The area A is the normal area to C_{mi}. For the rotor, it can be adapted to:

$$\dot{m} = \rho_i C_{mi} A_i \tag{1-9}$$

For the inlet of the rotor, knowing that b_1 is the inlet width of the blade and D_1 the rotor diameter, (1-9) can be evaluated resulting in equation (1-19).

$$\dot{m} = \rho_1 C_{m1} A_1 = \rho_1 C_{m1} \pi b_1 D_1 \tag{1-10}$$

For the outlet of the rotor, though, taking into account, from [11] that D_{2m} is designed approximately to be $0.5D_1$:

$$\dot{m} = \rho_2 C_{m2} A_2 = \rho_2 C_{m2} \pi b_2 D_{2m} = 0.5 \rho_2 C_{m2} \pi b_2 D_1 \tag{1-11}$$

1.3.5. The momentum equation

Based on the Newton's second law of motion, and applying it to the fluid passing through a control volume like in [10], the specific work transfer is given by:

$$\frac{\dot{W}}{\dot{m}} = U_1 C_{u1} - U_2 C_{u2} \tag{1-12}$$

For an outlet flow without swirl ($C_{u2} = 0$) and considering that $c_{u1} = 0.85u_1$ equation (1-12) is simplified to equation (1-13).

$$\frac{\dot{W}}{\dot{m}} = U_1 C_{u1} = 0.85 U_1^2 \tag{1-13}$$

Chapter 2: Real/Ideal Gas assumption effects (1D)

In this chapter the effects of the Ideal Gas assumption for R-245fa on the turbine expansion of an ORC process will be studied with a one-dimensional analysis. First, the variables that are necessary to model the gas will be explained. After that, the turbine geometry and its expansion will be described, and the needed parameters for the numerical calculations will be estimated. Finally, using a one dimensional design, the effects of the assumption will be evaluated.

2.1. Variables

2.1.1. Compressibility factor

The properties of gases are described by certain laws and generalizations concerning their behaviour. The main point is to know how pressure, volume and temperature are interrelated. The ideal gas laws describe only an idealized behaviour of the fluid, which is just an approach for real gases under certain conditions.

The ideal gas equation of state is:

$$pv = RT \tag{2-1}$$

And also:

$$p = z\frac{1}{v}RT = z\rho RT \tag{2-2}$$

p in N/m^2 is the absolute pressure of the gas, v in m^3/mol stays for the specific volume and T in K is the absolute temperature. R is the universal gas constant, 8.314472 J/Kmol multiplied by the gas molar mass M in mol/kg. According to [12], an ideal gas is a theoretical gas composed of a set of randomly moving, non-interacting point particles. At low pressures and/or high temperatures, the free space within the gas is large and the particles do not react significantly. Under these conditions, a real gas will approximate the ideal behaviour. Several hundred equations of state try to express the p-v-T relation, but none of these have been found universally satisfactory. In addition, the best of these equations are hard to work with and are used only when high accuracy is required.

The critical point of a substance indicates the maximum state value for which two phases can coexist in equilibrium. It represents the maximum temperature at which the gas can be liquefied by simply increasing its pressure. Reduced state variables are defined by their values, divided by the critical values of the substance.

$$p_R = p/p_c \; ; T_R = T/T_c$$

Different gases behave similarly at equal values of reduced temperature and pressure. This fact leads to a new concept, namely: The compressibility factor z, which represents a simple way to estimate real gas behaviour. It is a correction factor for the ideal gas to obtain a similar behaviour like a real gas:

$$p = z\frac{1}{v}RT = z\rho RT \tag{2-3}$$

This factor is set by the values of reduced temperature and reduced pressure. As it can be read in [13], it is independent of which real gas. When compressibility charts for different gases are studied, they are found to be qualitatively similar. Further study shows that when the coordinates are suitably modified, the curves for several different gases coincide closely when plotted together on the same coordinate axes, and so quantitative similarity also can be achieved. This is referred to as the principle of corresponding states.

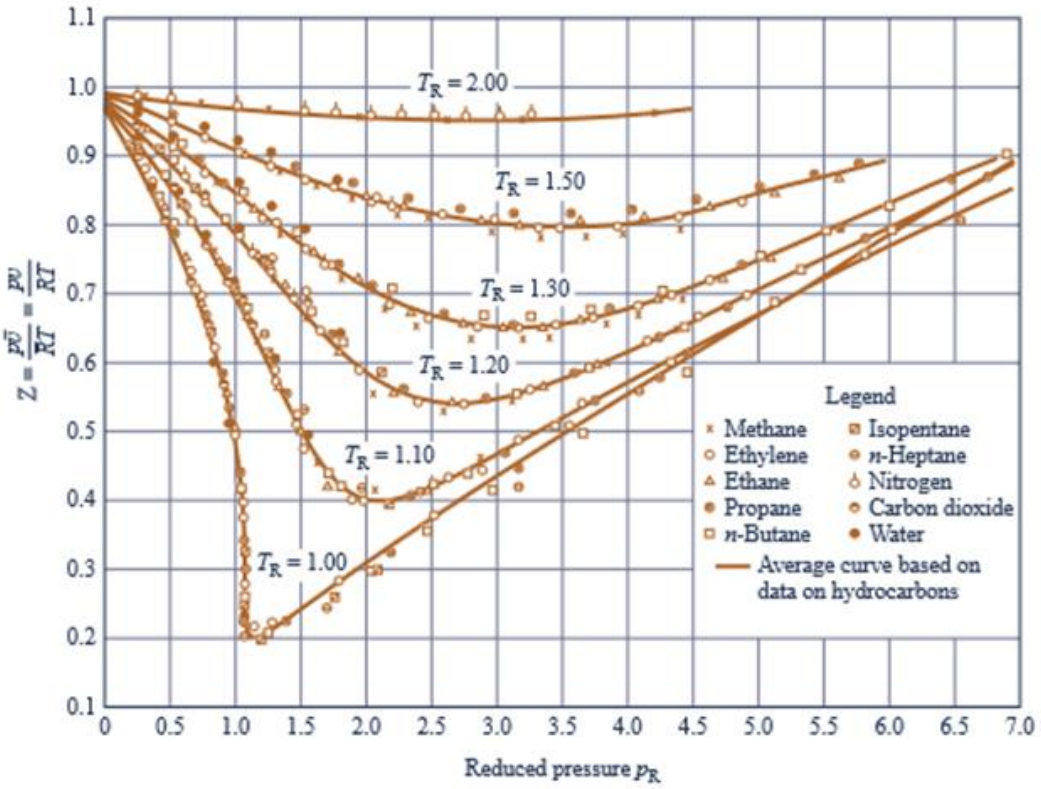

Figure 2.1: Compressibility chart for 10 different gases found in [13]

Figure 2.1 shows the experimental data for the compressibility factor using 10 different gases. The solid lines describe reduced isotherm. As commented, at pressures below the critical one or at very high temperatures, less error is committed when applying the ideal gas law. The chart helps to predict the deviation existing under different conditions and the evolution of the compressibility factor.

2.1.2. Heat capacities at constant pressure and constant volume

The heat capacity of a body is the ratio of the heat energy transferred to a body or system in a process and the temperature change experienced. It is the energy required to raise a unit of temperature of a substance. It indicates the degree of difficulty of a body to experience changes in temperature under a given heat supply.

Heat capacity at constant pressure, c_p in J kg^{-1} K^{-1} is the rate of change of enthalpy with respect to temperature, at a constant pressure:

$$\left(\frac{\partial h}{\partial T}\right)_p = c_p \tag{2-4}$$

The heat capacity at constant volume c_v has the same units as c_p. It is the rate of change of the internal energy with respect to temperature at constant volume:

$$\left(\frac{\partial u}{\partial T}\right)_v = c_v \tag{2-5}$$

2.1.3. Relation of enthalpy change to state conditions

Enthalpy change is one of the most important parameters when analysing the expansion process in a turbine. It is needed to calculate the efficiency of the process, which is the leading parameter when performing turbines.

Having a one-phase system of constant chemical composition, enthalpy depends on temperature and pressure:

$$h(T, p)$$

The differential change in enthalpy follows the expression:

$$dh = \left(\frac{\partial h}{\partial T}\right)_p dT + \left(\frac{\partial h}{\partial p}\right)_T dp \tag{2-6}$$

Using equation (2-5) and knowing that:

$$dh = Tds + vdp \tag{2-7}$$

Deriving and applying the Maxwell relations, like in [3], enthalpy change between two states can be calculated with the following expression:

$$\Delta h = \int_{T_1}^{T_2} C_p dT + \int_{p_1}^{p_2} \left[v - T\left(\frac{\partial v}{\partial T}\right)_p\right] dp \tag{2-8}$$

Enthalpy change can be written as:

$$\Delta h = \int_{T_1}^{T_2} C_p dT + \int_{p_1}^{p_2} \left[\frac{1}{\rho} - T \left(\frac{\partial \left(\frac{1}{\rho} \right)}{\partial T} \right)_p \right] dp \tag{2-9}$$

2.1.4. Adiabatic index

In thermodynamics, an adiabatic process is designated to one in which the system does not exchange heat with its surroundings. An adiabatic and reversible process is also an isentropic process.

The heat capacity ratio or adiabatic index or ratio of specific heats, is the ratio of the heat capacity at constant pressure to heat capacity at constant volume:

$$\gamma = \frac{C_p}{C_v} \tag{2-10}$$

And for an ideal gas:

$$\gamma = \frac{C_p}{C_p - R} \tag{2-11}$$

For an adiabatic process, there is no heat exchange between the system and the environment. This situation would be if there were a perfect thermal insulation of the system, or when the process happens so fast that there is almost no heat transfer possible. If the real gas is considered to behave as an ideal one, the combination of the first thermodynamic principle and the ideal gas equation of state provide a new concept: the adiabatic equation.

Applying the first law of thermodynamics:

$$dU = \delta Q - \delta W = \delta Q - pdV$$

For an adiabatic process $\delta Q = 0$ and using the differential ideal gas equation of state:

$$pdV + vdp = RdT \tag{2-12}$$

$$pV^{\gamma} = const. \tag{2-13}$$

$$p^{1-\gamma} T^{\gamma} = const. \tag{2-14}$$

Equation (2-14) will be very useful to know the adiabatic index for given operating conditions and to characterize an ideal gas.

2.2. Working properties and turbine geometry

The effects of the ideal gas assumption for a real gas will be investigated for a particular expansion and a particular turbine. Before going into the analysis, it is necessary to describe the expansion properties and the geometry of the turbine.

2.2.1. Working properties

The studied process is given by a turbine expansion of an ORC process. The working fluid is the refrigerant R-245fa and the operating properties of the expansion can be found in Table 2.1

Property	Value
Inlet temperature	85 $°C$
Outlet temperature	67 $°C$
Inlet pressure	8.5 bar
Outlet pressure	3.5 bar

Table 2.1: Operating properties of the expansion

A convenient way to observe the state values of the refrigerant during the process is locating the expansion on a pressure-enthalpy diagram.

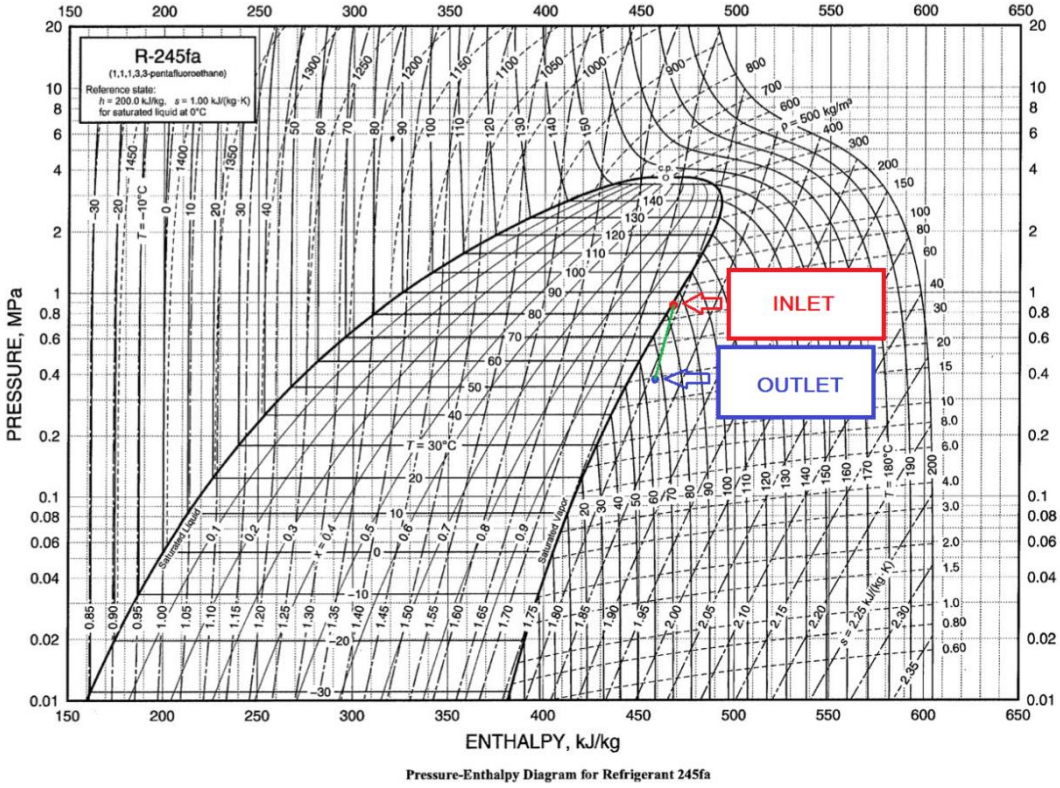

Figure 2.2: Expansion process of the ORC in the p-h diagram

The turbine expansion of the ORC can be ilustrated in Figure 2.2 in the p-h diagram of the refrigerant R-245fa. As it can be seen, the process takes place in the vapour zone, very close to the saturated vapour line.

	p $[MPa]$	T $[K]$	ρ $[kg/m3]$	h $[kJ/kg]$	s $[kJ/(kgK)]$
Inlet 0	0.85	358.15	49	466.5	1.979
Outlet 2	0.35	340.15	19	460	1.816
Ideal outlet state 2s	0.35	330.15	20	449	1.979

Table 2.2: Ideal state 2s regarded on the Pressure-Enthalpy Diagram for Refrigerant 245fa

Table 2.2 shows the thermodynamic properties and ideal states of the refrigerant at inlet and outlet. Knowing the outlet pressure, the ideal outlet state can be find out: It has the same entropy as the inlet state and the same pressure as the outlet state. An important deduction, that will help to analyse the expansion, is the ideal enthalpy change (h_0 - h_{2s}). This concept represents the maximal enthalpy change that the fluid would yield. The real process in the turbine though, is not isentropic and the efficiency will be calculated, like seen in the introduccion chapter, by comparing the real enthalpy change with this ideal one. For the given outlet pressure, the ideal enthalpy variation (h_0 - h_{2s}) has a value of 16.5 kJ/kg.

Other important working properties of the process are the rotational speed of the turbine, which is set to $\omega = 50000$ rpm, and the mass flow throw the turbine, which has a value of 0.215 kg/s.

2.2.2. ITSM turbine geometry

The ITSM provided a turbine model, which was designed for the mentioned working conditions. From now on, this turbine will be called “Turbine 1”. Knowing its dimentions, it will be possible to predict and compare real gas with ideal gas state values. Through this comparison it will be possible to determine if the ideal gas assumption is acceptable or not.

The blade is the foundation of the radial turbine geometry. The one dimensional design of radial is based on its blade dimensions. Figure 2.3 helps to be conscious of what each turbine dimension really means:

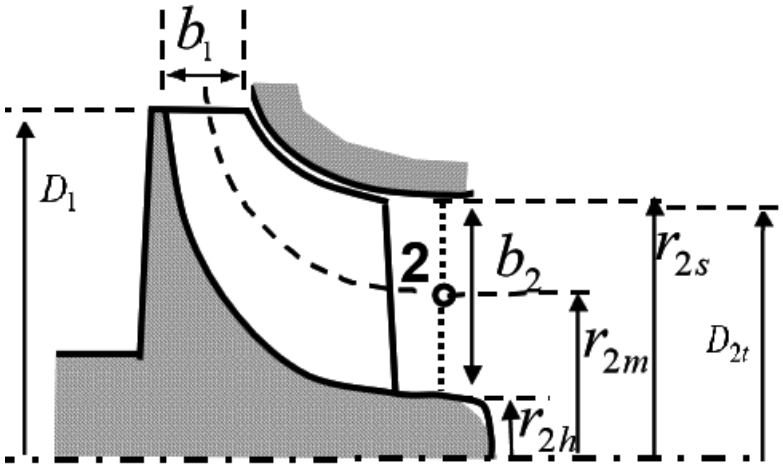

Figure 2.3: Meridional projection of the blade from [11]

The subindex “h” stands for hub, and “s” stands for shroud. The hub is where the blade originates. The shroud is the non rotating wall that forms the duct together with the hub. There can not be any contact between shroud and blade. Therefore a tip gap is located between the blade tip and the shroud wall.

The blade of turbine 1, has the geometrical characteristics shown in Table 2.3.

	D_1	b_1	b_2	r_{2s}	r_{2h}	D_{2t}
Blade	48	2.7	11	18.2	7.2	36.2

Table 2.3: Geometrical properties of the blade in [mm]

In order to perform the one dimensional design that will reveal the ideal gas assumption effects, the different areas through the turbine are needed and can be calculated as follows:

Inlet area of the stator can be calculated as:

$$A_0 = \pi D_0 b_0 = \pi D_0 b_1 = 661.62 \cdot 10^{-6}\ m^2$$

Where the stator inlet diameter D_0 has a value of 0.078 m.

The rotor inlet area can be calculted the same way:

$$A_1 = \pi D_1\, b_1 = \pi D_1 b_1 = 424.11 \cdot 10^{-6}\ m^2$$

Finally, the rotor outlet area, since it is a ring with inner radius r_{2h} and outer radius r_{2s} can be estimated as:

$$A_2 = \pi\left(r_{2s}^2 - r_{2h}^2\right) = 877.76 \cdot 10^{-6}\ m^2$$

2.3. Estimation of the parameters for the simulations

The ITSM provided an excel file with R-245fa state values. The variables included are: absolute temperature, absolute pressure, density, enthalpy and entropy. The first step in analysing the data is to know the nature of the data. Figure 2.4 is a representation of the data in a Pressure-Enthalpy diagram.

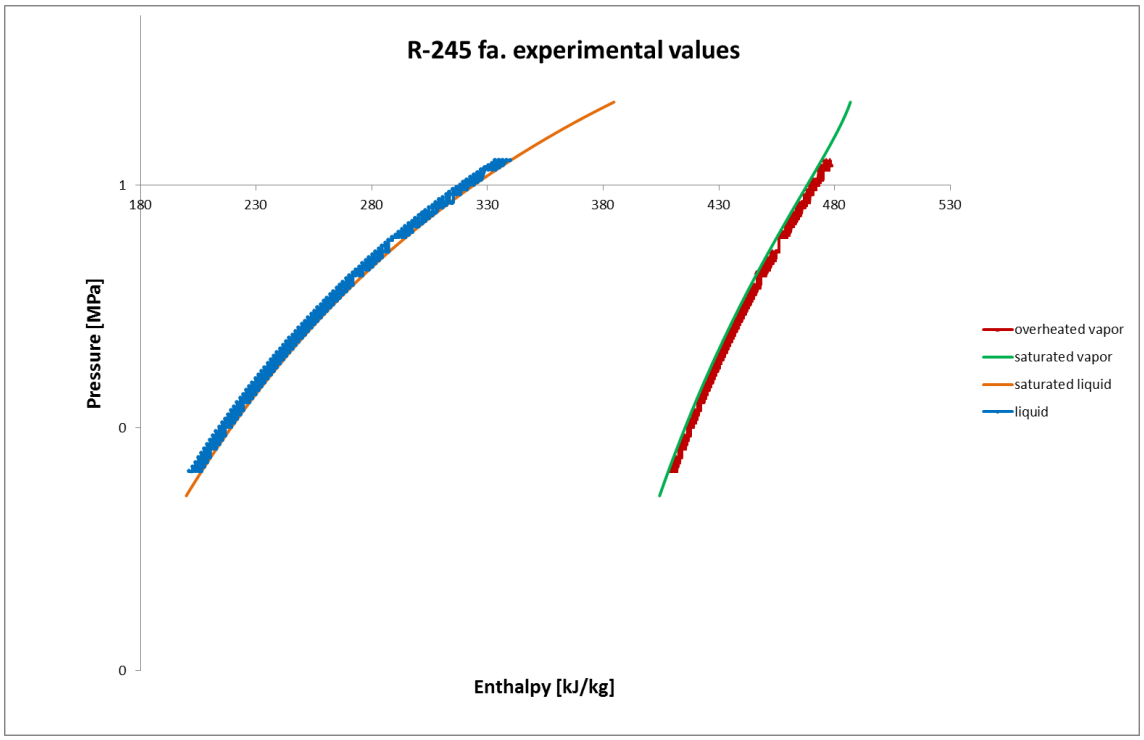

Figure 2.4: Representation of the excel data in a p-h diagram

The data locates at 4 different areas: The liquid area, the saturated liquid line, the saturated vapour line and the vapour area. Thanks to the saturated vapour line, it is easy to decide the values that will be studied in detail: The vapour values, which can be found to the right of the line. The turbine works in the vapour area of the diagram, so it makes no sense to take into account values in the bell or on its left.

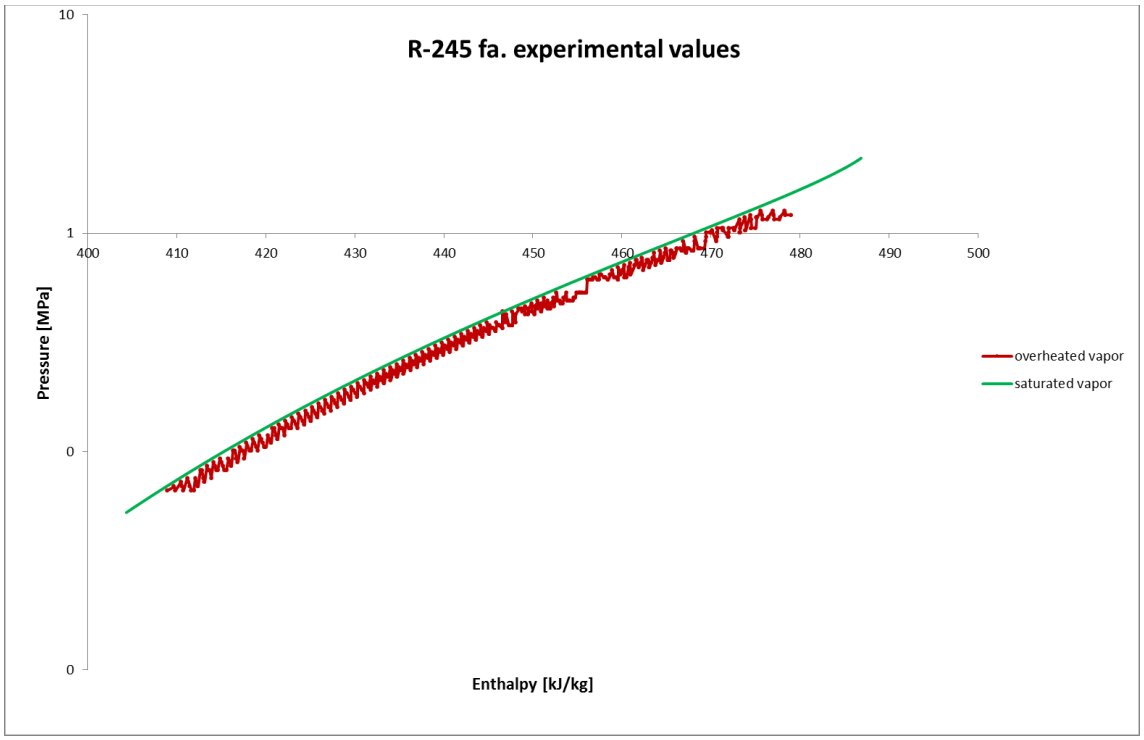

Figure 2.5: View of the vapour data in the p-h diagram

Figure 2.5 shows that for each pressure value, there are around four values four vapour state. These values will help to evaluate the variables are needed for the simulation.

A new range of study will be considered: The one carried out in the expansion of the ORC. The data concerning temperature between $[88°C\ ;\ 62°C]$ or $[361{,}15\ K;\ 335{,}15\ K]$. That entails a reduced temperature of $[0{,}78\ ;\ 0{,}85]$ and a reduced pressure of $[0{,}12\ ;\ 0{,}25]$. The reason for choosing this range of study is because it approaches the range of the real turbine process in ORC applications.

2.3.1. Real gas parameters

An important parameter for the real gas simulation is the heat capacity at constant pressure. In order to calculate it, the best way is using its definition (2-4).

If data is classified by decreasing pressure, c_p can be calculated for each four points with exactly the same pressure. That would be a perfectly isobaric process. For each two consecutive data values with same pressure, c_p is calculated as:

$$\frac{\Delta h}{\Delta T} = c_p \qquad (2\text{-}15)$$

As a result, c_p can be plotted in relation to temperature to investigate its dependency on it:

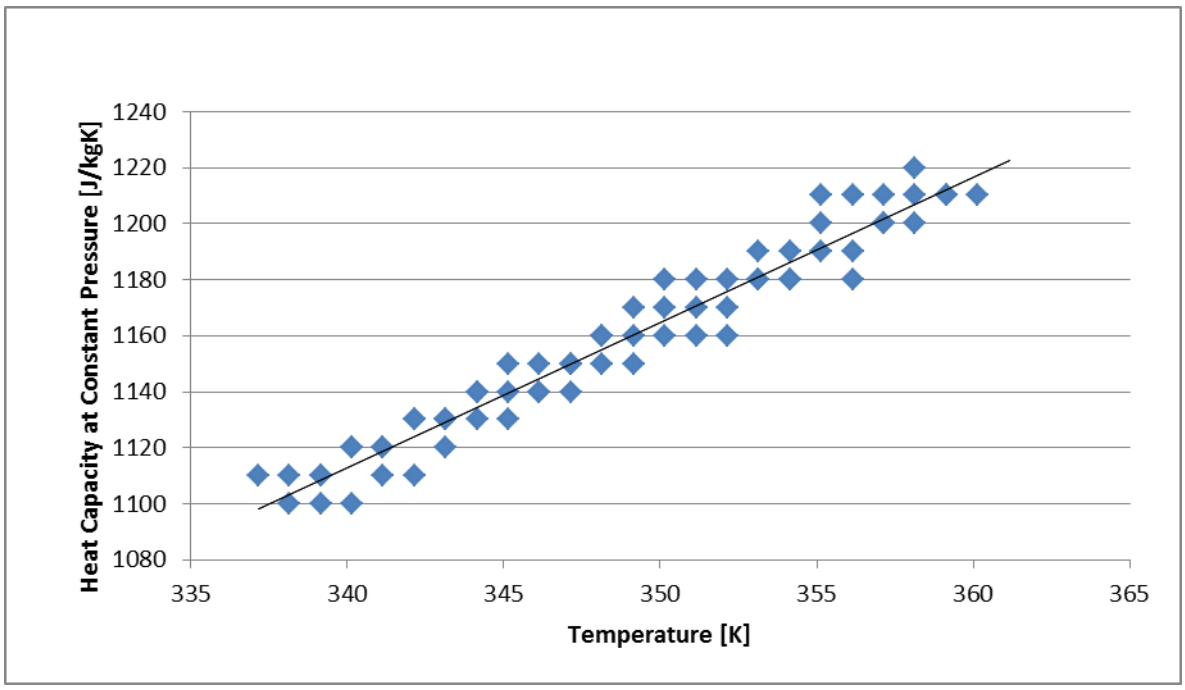

Figure 2.6: Representation of the heat capacity C_p depending on the temperature

c_p seems to be dependent on temperature as it is shown in Figure 2.6. In order to calculate enthalpy change, it is easier to consider it as constant. The error committed is less than a 5% when considering it to have a constant value of 1156.786 J kg^{-1} K^{-1}, which is the average of the data.

2.3.2. Ideal gas parameters

For a real gas, the second term of equation (2-8) gains consideration under conditions, where the real gas does not approach the ideal gas law. It will be now investigated whether it has to be considered for the field of the turbine expansion of the ORC.

Enthalpy lines in the p-h diagram are vertical lines. Applying the enthalpy equation (2-8) it is deductible, that isenthalpic processes imply isothermal processes. Therefore, if R-245fa was an ideal gas, the isothermal lines of the p-h diagram would be vertical for the gas region. The fact that they do not, is because of the second term of equation (2-8).

If the values of the working parameters of Table 2.1 are considered and contemplating a c_p of 1156.786 J kg^{-1} K^{-1}, the enthalpy variation of the process, not considering the second term of equation 2-8, can be calculated as:

$$\Delta h = \int_{T_1}^{T_2} C_p dT = C_p(T2 - T1) = \frac{1156J}{kgK} \cdot (358.15 - 340.15) = 20.8kJ/kg$$

At the p-h diagram though, a variation in enthalpy of about 6.5 kJ/kg can be read directly for this process. This would represent an error when calculating enthalpy change of more than a 200%.
The second term of equation (2-8) has to be taken into account. When considering ideal gas law, the second term goes to zero and the c_p of the real gas deals to a wrong value of enthalpy change. It can be also concluded, that the ideal gas law for the field of study will lead to a wrong relationship between enthalpy variation and temperature variation and to a wrong simulation when using the same heat capacity at constant pressure as the one used for the real gas simulation.

A possible way of modelling R-245fa for this process is also to adapt the value of c_p to the conditions of the expansion.

On this account, a possible way of modelling the refrigerant as an ideal gas is to, considering an enthalpy variation value of 6.5 kJ/kg, calculate the c_p value with equation (2-15). Knowing that the enthalpy change takes place for at 18.2 K temperature change:

$$C_p = \frac{\Delta h}{\Delta T} = \frac{6500\ J/kg}{18.2\ K} = 357\frac{J}{kgK}$$

Since the enthalpy variation equation fits for the field of the project, it is interesting to run such a simulation and interpret the results. From a thermodynamic point of view it is rational.

2.4. Ideal gas assumption effects

The compressibility factor is the basis of the ideal gas assumption effects analysis.

In order to know reduced variables, it is necessary to have knowledge of the critical pressure and temperature of R-245fa. According to the National Institute of Standards and Technology (NIST) in [9], R-245fa has the critical properties presented in Table 2.4.

Critical pressure p_c $[MPa]$	3.64
Critical temperature T_c $[K]$	389.96

Table 2.4: Critical pressure and temperature of R-245fa

For the range of the simulation, an overview of the reduced pressure values using the excel data can be plotted:

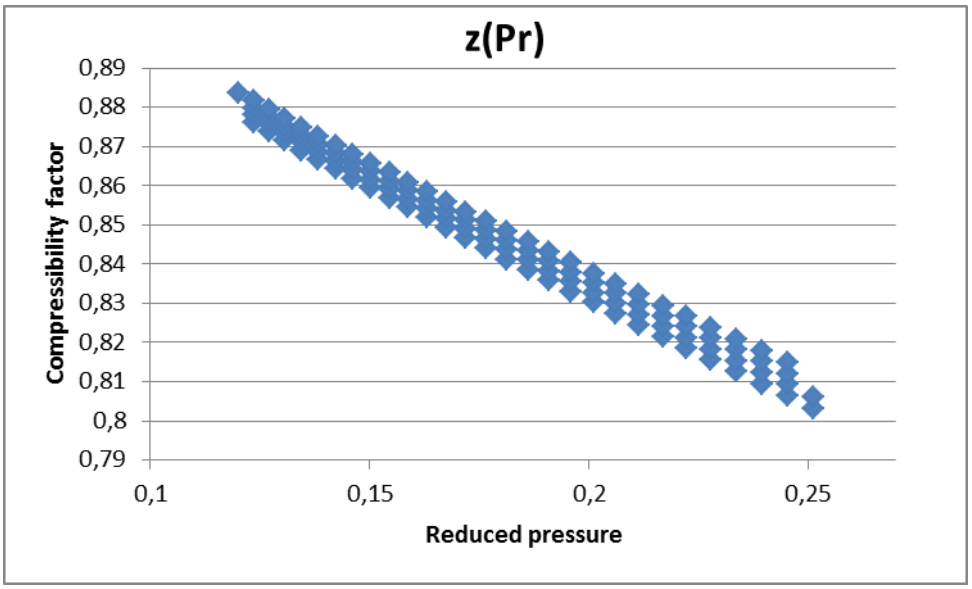

Figure 2.7: Compressibility chart for the expansion

As it can be seen in Figure 2.7, the compressibility factor has a range of [0.87-0.82]. The inlet pressure is nearer to the critical value and has a lower compressibility factor value, while the outlet, having a lower pressure, shows a lower value.

Compressibility factor indicates a deviation from ideal gas behaviour. The impact of this deviation will be analysed in the following lines:

Knowing the compressibility factor of the excel file, the state value deviations can be calculated.

	Inlet	**Outlet**
$p\ [MPa]$	0.85	0.35
$T\ [K]$	358.15	340.15
$\rho\ [kg/m^3]$	46	19
$z = p/TR\rho$	0.83	0.87

Table 2.5: Compressibility factor calculation of the inlet and the outlet of the expansion

The compressibility factors of Table 2.5 show a significant deviation from ideal gas behaviour, which can be studied analytically. For the inlet, when simulating the boundary conditions, pressure and temperature are set to their values of Table 2.5. The density for R-245fa working as an ideal gas can be calculated by applying ideal gas equation of state (2-1).

For an ideal gas, a value of 38.2 kg/m^3 is calculated. As for the inlet, the compressibility factor is equal to 0.85, R-245fa modelled as a real gas will have a value of 46.02 kg/m^3.

Applying continuity equation (1-9), the meridional velocity at inlet of the stator for the ideal simulation can be calculated as:

$$c_{m0} = \frac{\dot{m}}{\rho_0 A_0} = \frac{0.215\ \frac{kg}{s}}{38.2\ \frac{kg}{m^3} \cdot 661.62 \cdot 10^{-6}\ m^2} = 8.5\ \frac{m}{s}$$

Knowing that the flow enters the stator with an angle of 70°, the absolute velocity at inlet of the stator is:

$$c_0 = \frac{c_{m0}}{\cos(70º)} = 24.87 \frac{m}{s}$$

The enthalpy variation between a static and a total state can be calculated, like explained in the Introduction chapter, as:

$$h_{t0} - h_0 = \frac{1}{2} c_0^2 = \frac{1}{2}\left(24.87 \frac{m}{s}\right)^2 = 309.26 \frac{J}{kgK}$$

The same process can be repeated but for the real gas density. Table 2.6 shows the errors committed by assuming ideal gas behaviour.

	Ideal gas	Real gas	Error [%]
Inlet density [kg/m^3]	38.2	46.02	17
Inlet absolute velocity [m/s]	24.87	20.64	17
$h_{t0} - h_0$ [$J\ kg^{-1}\ K^{-1}$]	309.26	213.05	45.16
Efficiency [%]	-	-	0.58

Table 2.6: Ideal gas assumption errors at inlet

The errors committed when calculating the difference between total and static inlet enthalpy seem to be very high. The efficiency of the cycle is one of the most important parameters when analysing a turbine expansion. As it can be seen in table 5, a difference of (309.26-213.05) in front of an ideal enthalpy change of 16.5 kJ/kg causes an error on efficiency calculation of 0.73%, which can be accepted.

	Ideal gas	Real gas	Error [%]
Outlet density [kg/m^3]	16.59	19	12.68
Outlet absolute velocity [m/s]	23.344	18.5	20.75
$h_{t2} - h_2$ [$J\ kg^{-1}\ K^{-1}$]	272.47	171.25	37.2
Efficiency [%]	-	-	0.58

Table 2.7: Ideal gas assumption errors at outlet

The same procedure can be applied to the outlet. Table 2.7 shows also a very low error expected when calculating the total efficiency. In fact, it is lower than at the inlet of the stator, because the pressure is smaller and the gas approaches more the ideal behaviour.

It was proofed, that the ideal gas assumption entails a change in state values and it produces effects on the velocities and so, on the enthalpy variation and on the efficiency. For this reason it is very important to evaluate these effects at the rotor inlet, where absolute velocities have higher values:

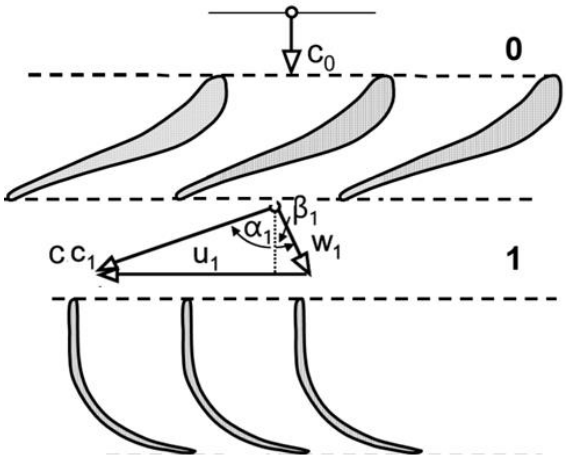

Figure 2.8: Rotor inlet triangle of velocities

Inlet velocity triangle can be observed in Figure 2.8. As seen in Introduction, the turbine is designed to have an absolute velocity angle α_1 of 70° and an incidence factor, $\frac{c_{u1}}{u_1}$, of 0.85. The rotational speed u_1 can be calculated for the turbine analysed in this part of the project by knowing its rotor angular speed.

$$u_1 = \omega \frac{D_1}{2} = 50000\ rpm \cdot \frac{\pi\ s^{-1}}{30\ rpm} \cdot \frac{0.050\ m}{2} = 130.9\ \frac{m}{s}$$

Working at the designed characteristics, the different velocity components at rotor entry can be calculated.

$$c_{u1} = 0.85 \cdot 130.9\ \frac{m}{s} = 111.265\ \frac{m}{s}$$

$$c_{m1} = 111.265\,\frac{m}{s} \cdot \frac{1}{\tan 70º} = 40.497\,\frac{m}{s}$$

$$c_1 = \frac{c_{u1}}{\sin 70} = 118.406\,\frac{m}{s}$$

$$w_{u1} = u_1 - c_{u1} = 19.63\,\frac{m}{s}$$

$$w_1 = \sqrt{w_{u1}^2 + c_{m1}^2} = 45\,\frac{m}{s}$$

$$\beta_1 = \sin^{-1}\left(\frac{w_{u1}}{w_1}\right) = 25.87°$$

The meridional velocity is related with the density by the continuity equation (1-10). At inlet both simulations will have the same temperature and pressure. This leads to a density deviation.

Ideal and real gas simulations will have the same mass flow and the same area at rotor inlet. Because of that, their meridional velocities will differ by the same proportional factor as the densities, just in an inverse way; ideal gas meridional velocity will be higher as the real gas one.

Both simulations have the same stator. Presuming, therefore, a constant angle α_1 at rotor inlet, the velocity triangles will differentiate like Figure 2.9 shows.

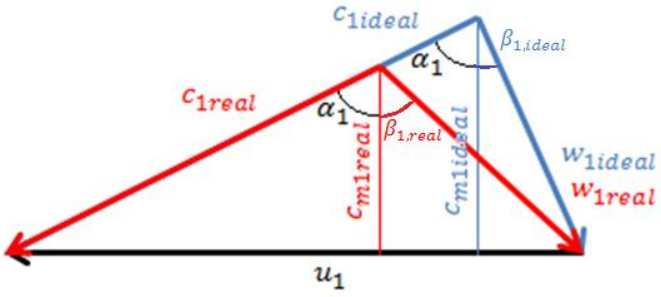

Figure 2.9: Rotor inlet expected velocity triangles

Figure 8 manifests the remarkable differences expected between both simulations. The lower absolute velocity of the real gas leads to a higher relative velocity component and to a more obtuse relative angle β_1. Considering, that the quotient between ideal density and real density remains constant along the stator.

$$\frac{\rho_{1,real}}{\rho_{1,ideal}} = \frac{\rho_{0,real}}{\rho_{0,ideal}} = z_0 = 0.83$$

The real gas simulation velocities at rotor entry can be calculated. The expectations can be seen in Table 2.8.

Variables	Ideal gas simulation	Real gas simulation	Error [%]
u_1 [m/s]	130.9		-
α_1 [°]	70		-
c_{m1} [m/s]	40.497	33.61	20.5
c_1 [m/s]	118.406	98.28	20.5
$\frac{C_{u1}}{U_1}$	0.85	0.71	19.7
w_1 [m/s]	45	51.14	12
β_1 [°]	25.87	48.91	47

Table 2.8: Velocity rotor inlet triangle components expected for both simulations

Two important conclusions can be drawn from Table 2.8. The first conclusion has to do with the incidence factor. According to [11], the optimum value is 0.85. This factor depends on the blade number Z, like [15] pioneered.

$$-\frac{C_{u1}}{U_1} = 1 - 0.63\frac{\pi}{Z} \tag{2-16}$$

If the expected ideal has an incidence factor of 0.85, the real gas simulation will exhibit a lower value entailing approximately a 20%. Therefore, the entry in the rotor for the real gas will differ from the entry of the ideal gas. The real gas is expected to have a worse entry in the rotor, which implies more losses through the rotor and a lower efficiency than the ideal gas.

The other important conclusion to be taken up to this point is that the change in absolute rotor inlet velocity c_1 will trigger an important stator enthalpy change.

$$h_{t1} - h_1 = \frac{1}{2}c_1^2 = 6400\ \frac{J}{kg}$$

The absolute velocity c_1 expected for the ideal gas simulation leads to an enthalpy change through the stator of 6400 J/kg. Following table shows the possible difference between rotor inlet enthalpies for the ideal and the real gas considering a compressibility factor of 0.86.

Gas type	Velocity c_1 [m/s]	Total-static enthalpy change Δh_1 [kJ/kg]
Ideal	118.406	7010
Real	98.28	4829

Table 2.9: Rotor inlet enthalpy variation as a consequence of ideal gas assumption

Enthalpy variations differ in 2181 J kg^{-1} K^{-1} and it will have an effect on the efficiency calculation. In order to evaluate the effect of the variation on the total to static efficiency, the rotor enthalpy can be considered equal to both simulations and the effects of the enthalpy change deviation can be exposed for different values of rotor enthalpy change, as it presents Figure 2.10.

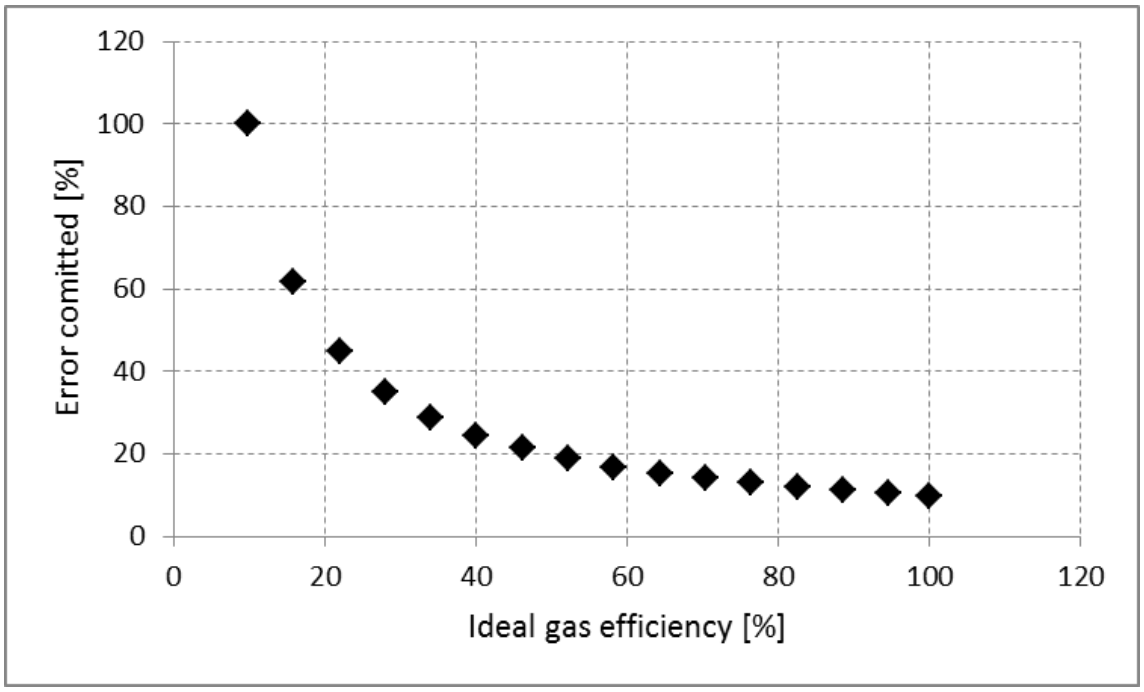

Figure 2.10: Error on total to static efficiency considering same rotor enthalpy change

The stator enthalpy change deviation has an important effect on total to static efficiency. Knowing from the first conclusion announced that the rotor enthalpy change will be different for each simulation; the error committed showed in figure 9 will be even higher, but it helps to realize the important efficiency deviations that at least exist just because of the stator enthalpy change deviation.

2.5. Summary

Using an ideal gas model implies that the second term of the enthalpy change equation (2-8) is assumed to be zero. For a range of low pressures it would be an acceptable hypothesis. The range can easily be recognized where the isothermal lines in the p-h diagram are vertical. The fact that they bend for pressures above 0.1 MPa close to the saturated vapour line, indicates a deviation from ideal gas behaviour and an important error when applying equation (2-9). This equation is also not valid for the c_p value of 1156 J kg^{-1} K^{-1}, which is the c_p value calculated for the real gas R-245fa. Based on the enthalpy change needed by the refrigerant to reach the outlet temperature and pressure, a heat capacity at constant pressure of 357 J kg^{-1} K^{-1}s et on for an ideal gas simulation can lead to the expected working properties of Table 2.1.

The pressures of the expansion analysed in this thesis seem to be too high to consider an ideal behaviour of R-245fa, despite adapting the heat capacity at constant pressure value to the expansion enthalpy change of the real gas.

When performing the one dimensional design, an important density deviation is expected between the real gas and the ideal gas. This deviation, applying the continuity equation, leads to a proportional absolute velocity deviation. A lower value of rotor inlet absolute velocity causes an enthalpy change variation in the stator. It also has an effect on the rotor inlet relative velocity and its direction, which will occasion a different entry in the rotor. This issue could involve supplementary losses through the rotor that would mean a decrease of enthalpy change in the rotor. These two facts suggest a lower efficiency value for the real gas simulation. The efficiency variation suggests that the ideal gas model defers overmuch to the ideal gas model and will not be a good approximation.

Chapter 3: Real/Ideal Gas assumption effects on ANSYS CFX

In this chapter, the results from the two simulations carried out for the topic “Real/Ideal Gas assumption effects” will be presented and discussed. The first thing explained is the modelling of the turbine. Afterwards, the results of the numerical calculations will be exposed and discussed by comparing them to the predictions of the theory chapter. It will then be decided which of the models is valid and can be used to perform the optimitazion .

3.1. Setting on the simulations

3.1.1. Geometry and meshing

The geometries of the turbines calculated in the project were given by the ITSM. The turbine, for which the ideal gas assumption effects will be investigated, will be named in this chapter “Turbine 1”. Turbine 1 consists on a stator and a rotor. The stator has 11 guide vanes and the rotor has 12 blades. Figure 3.1 shows the geometry of the turbine.

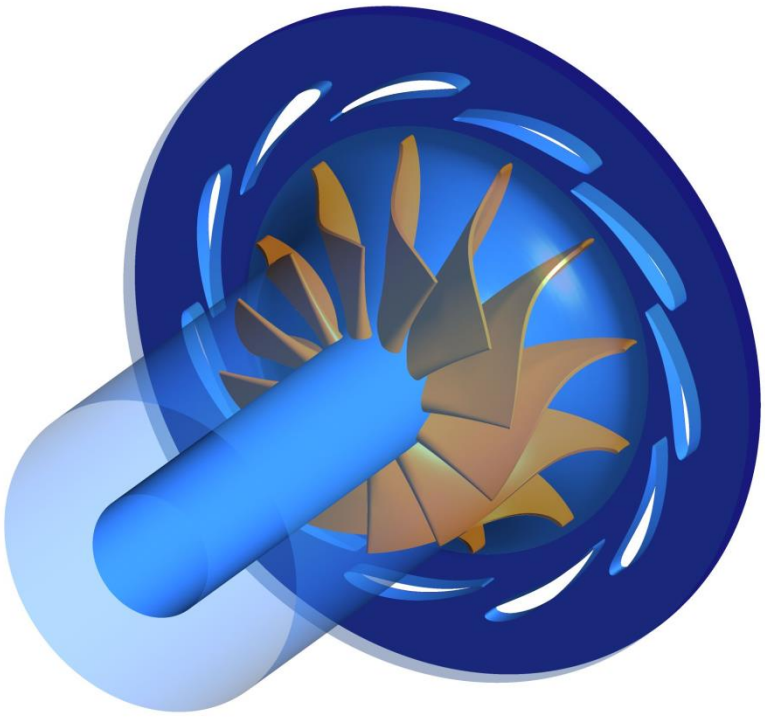

Figure 3.1: Geometry of the turbine (ANSYS CFX-Post)

The twelve blades seen in Figure 3.1 compose the rotor of Turbine 1. The eleven guided vanes form its stator.

Table 3.1 shows the geometric properties of the turbine.

[mm]	D_1	b_1	b_2	r_{2s}	r_{2h}
Turbine 1	48	2.7	11	18.2	7.2

Table 3.1: Geometrical properties of the turbine 1 in [mm]

The blades of Turbine 1 where designed to have a radial orientation at inlet; at outlet, blade angles of -60° to -70° as found in [10]. These are typical characteristics of radial inflow turbines.

Meshing process of Turbine 1 was carried out using ANSYS TurboGrid software. This software is used to import geometry definitions from blade design softwares. Selected topologies are adjusted to the specifics of a particular blade design. Once the geometry is meshed, an output file compatible with ANSYS CFX can be created.

As meshing of Turbine 1 was carried out by the ITSM, the different meshing steps will not be explained for the simulations of this chapter. Chapter 4 will show a meshing process.

3.1.2. Pre-processing with ANSYS CFX-Pre

With ANSYS CFX-Pre all wished working conditions and properties are applied to the geometry resulting from ANSYS Turbogrid.

3.1.2.1. Domains

The concept of domain defines the type, properties and region of the fluid. Domains are regions of space in which the equations of fluid and heat transfer are solved. A domain can be stationary or rotating and that is the reason why in order to simulate the turbine, two separated domains are needed: A stationary one for the stator (S1) and a rotating one for the rotor (R1), which includes the passage of the rotor and the outlet, as it can be seen in Figure 3.2.

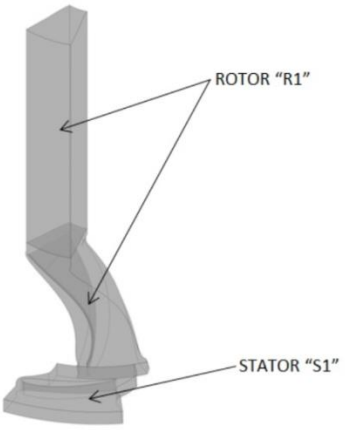

Figure 3.2: Domains of turbine 1

The different characteristics of both domains are explained in the following lines:

- Domain type: For both domains the fluid domain option is selected. It is the only one which allows working with just one fluid.

- Morphology: The best option for both domains is the continuous fluid, because the fluid is not a particle phase, but an Eulerian one.

- Reference Pressure: Reference pressure for both domains is set to 0 MPa.

- Bouyance Model: This model takes into account the gravitational effects. For these simulation, they are, compared to kinetic effects, not to be taken into account. That is the reason why that option is discarded for both domains.

- Heat transfer: In turbine simulations the kinetic effects are the most important ones. Total energy option models the transport of enthalpy and includes kinetic energy effects. It is then the best option.

- Turbulence: R1 and S1 share turbulence model, namely: Shear Stress Transport. The SST k-ω turbulence model is a two-equation eddy-viscosity model which has become very popular. According to [22], the shear stress transport (SST) formulation combines the best of both models. The use of a k-ω formulation in the inner parts of the boundary layer makes the model directly usable all the way down to the wall through the viscous sub-layer, hence the SST k-ω model can be used as a Low-Re turbulence model without any extra damping functions. The SST formulation is also switched to a k-ε behaviour in the free-stream and thereby avoids the common k-ω problem that the model is too sensitive to the inlet free-stream turbulence properties. Authors who use the SST k-ω model often merit it for its good behaviour in adverse pressure gradients and separating flow.

In addition, “R1” and “S1” do not consider any combustion or thermal radiation option or electromagnetic models, because the turbine expansion does not submit such effects.

3.1.2.2. Interfaces

Thanks to the use of interfaces the computing machine can run the simulation and its calculations regarding only a fraction of the turbine. The simulation will be computed for just a fraction containing one guided vane and one rotor blade. The results of the other fraction, being radially symmetric, will not be calculated but repeated from the computed one. Simulating a fraction and not the whole turbine saves relieves the calculations needed and alleviates the simulations.

Interfaces are also needed to match regions with non-coinciding mesh. Four interfaces are required in the pre-processing, namely: One for the rotor, “PerR1”, to match the 12 fractions of the rotor; one for the stator, “PerS1”, to match all 11 fractions of the stator; one for the matching between rotor and stator, “S1R1”; and one for the shroud tip, “TipGapR1”. The different options that describe the Interfaces are:

- Interface Type: All of the named interfaces are Fluid to Fluid, since all of them connect two fluid domains or make a periodic connection between two regions in a fluid domain.

- Interface Models option: For the interface between rotor and stator and the one used for the shroud tip, the interface models option is set to General Connection, because they connect non-matching grids. For the interfaces between the 12 different fractions a rotational periodicity is chosen.

- Mesh Connection: In the case of the interface between rotor and stator and the one used for the shroud tip, the mesh connection selected is GGI (General Grid Interface). That option is necessary when the grid on either side of the two connected surfaces does not match. For the interfaces between the different fractions the 1:1 option can be set, since the grids that they bound match.

3.1.2.3. Boundary conditions

To solve the calculation, it is necessary to define an operating point. Therefore boundary conditions are needed. They must be applied to all the bounding regions of the domains. Boundary conditions can be set at inlets, outlets, openings, walls, symmetry planes and interfaces. Utilized boundary conditions are explained in the following lines, grouped in the different types.

- Inlet boundary

The flow regime at inlet is expected to have a Mach Number below the unity. That is the reason why for inlet boundary a subsonic flow regime is chosen. Velocity at inlet, as commented in the Introduction, will be low enough to consider both states, total and static, the same. That is the reason why for both “Inlet” boundaries the total pressure will be set to 0.85 MPa as boundary condition. Because of the higher velocity expected for the ideal gas simulation, its total temperature will be set to 359.15 K and not 358.15 K like for the real gas one. The first assumption to validate when analysing the results from the simulations is therefore to verify that the static state at inlet does not have an important deviation from the total one.

The flow direction is set by an inlet absolute flow angle of 70°, which is a proper value for the fluid coming from a volute. The best turbulence option is medium, since it is the recommended option if one does not have any information about the inlet turbulence.

- Outlet boundary

The outlet flow regime is also set to subsonic and the mass flow rate has to be set to 0.0179166 kg/s, which is the twelfth part of the total mass flow rate 0.215 kg/s. The reason for dividing to 12 is because the outlet area is a fraction of the total. The fraction is given by the number of rotor blades, 12.

- Wall boundaries

Boundaries seen in Figure 3.3 and Figure 3.4: “Blade”, “Hub”, “HubOut”, “Shroud”, “ShroudOut”, “HubS1”, “ShroudS1” and “Vane” regions are wall type boundaries. All of them are set to No Slip wall, Smooth Wall and adiabatic. The walls are adiabatic, so that no heat exchange with the outside is considered and the process becomes an adiabatic one. When selecting No Slip Wall option, the fluid immediately next to the wall assumes its velocity. “Blade”, “Hub”, “HubOut”, “Shroud” and “ShroudOut” are rotating because of the rotating domain “R1”, but wall velocity of “HubOut”, “Shroud” and “ShroudOut” is chosen to be counter-rotating. This option sets their velocity to zero.

- Interface

“PerR1 Side 1”, “PerR1 Side 2”, “S1R1 Side 1”, “S1R1 Side 2”, “TipGapR1 Side 1”, “TipGapR1 Side 2”, “PerS1 Side 1” and “PerS1 Side 2” are boundary conditions that appear by default when creating the interfaces.

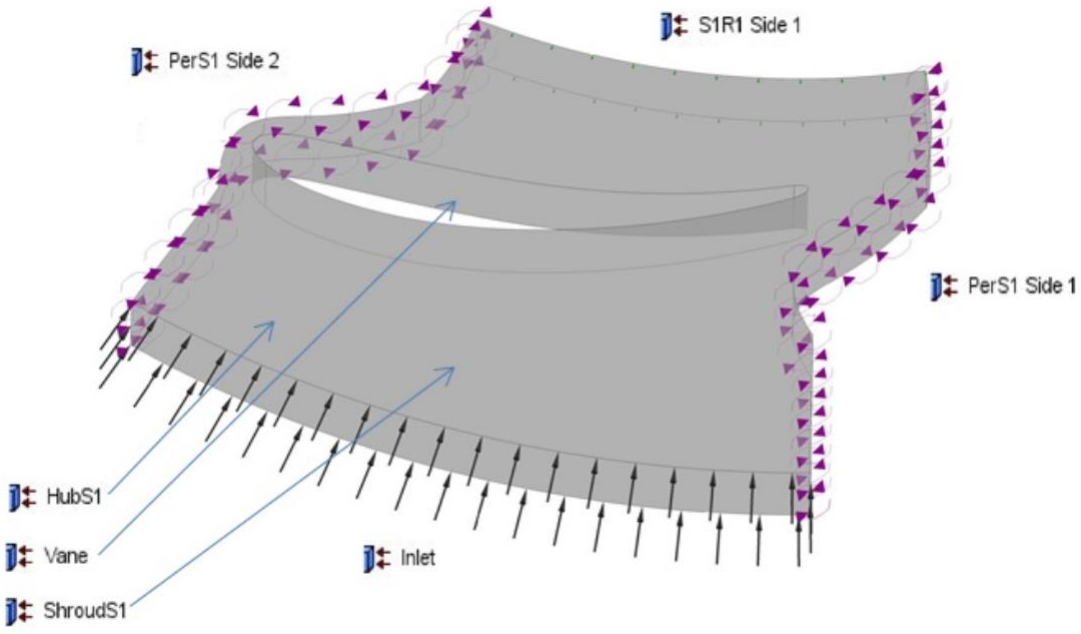

Figure 3.3: Stator domain and its boundary conditions

The black arrows in Figure 3.3 indicate the inlet boundary condition. “Vane”, “ShroudS1” and “HubS1” are wall boundary conditions. All the other are boundary conditions from the interfaces. As it can be observed, these interface boundary conditions are needed to match other fractions of the stator to the one seen in Figure 3.3.

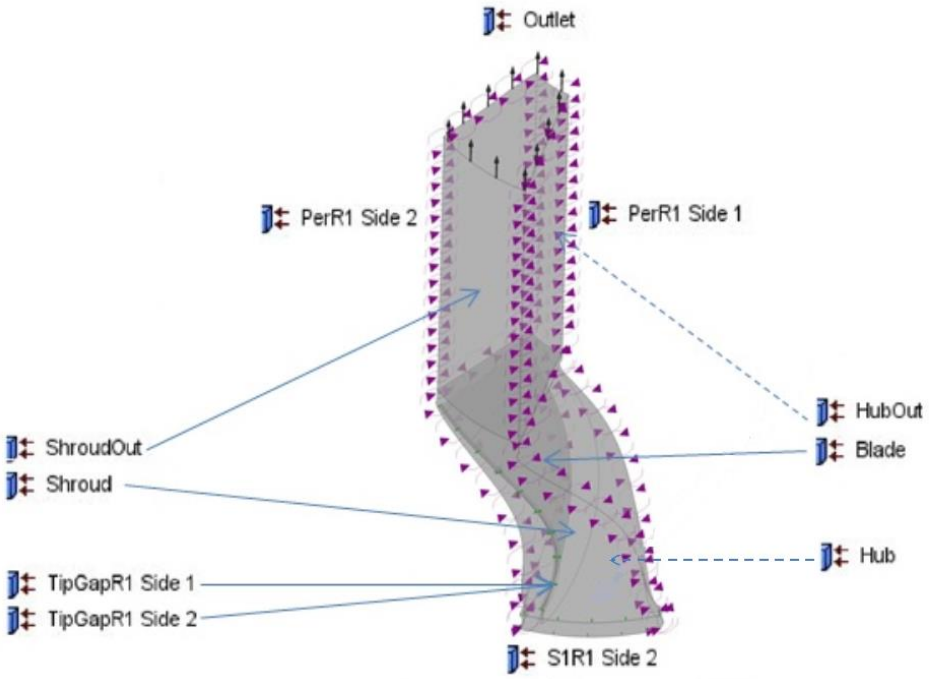

Figure 3.4: Rotor boundary conditions

The black arrows of Figure 3.4 designate the outlet boundary condition. “Blade”, “Hub”, “Shroud”, “ShroudOut” and “Hubout” are wall boundaries; the rest are default boundary conditions introduced by the interfaces.

3.1.2.4. Materials

One of the basic reasons for this study is to find a way of simulating R-245fa. There are three ways of simulating a gas in ANSYS CFX:

- Using the built in Ideal Gas equation
- Using the built in Real Gas equations
- Reading properties from a CFX-TASCflow RGP table

Two simulations are executed in Chapter 3: One with an ideal gas model and one with a real gas model.

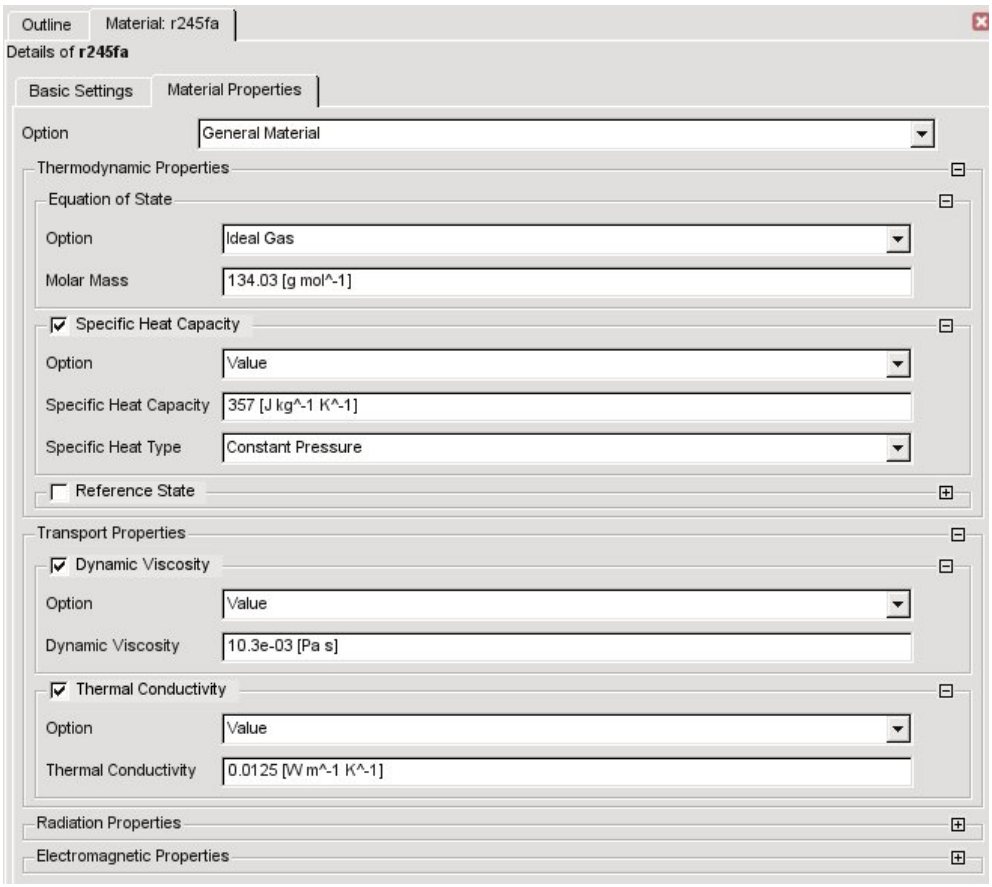

Figure 3.5: Ideal gas simulation material Properties in ANSYS CFX-Pre

Figure 3.5 shows the material properties tab integrated in ANSYS CFX-Pre simulating R-245fa for the ideal gas simulation. The molar mass will be the same for both simulations, since the atomic formula does not change. Its value, as shown by Figure 1.4, is set to 0.134 kg/mol.

For the specific heat capacity option, a constant heat capacity at constant pressure value is chosen. The reason for this value is mentioned in Chapter 2; it is based on the expected enthalpy change and temperature change for the expansion.

Finally, the dynamic viscosity and the thermal conductivity can be found thanks to NIST data found in [9]. The real gas material properties tab from ANSYS CFX-Pre requires more inputs, as it can be seen in Figure 3.6. The critical state values can be found using [9], as well as the acentric factor and the boiling temperature.

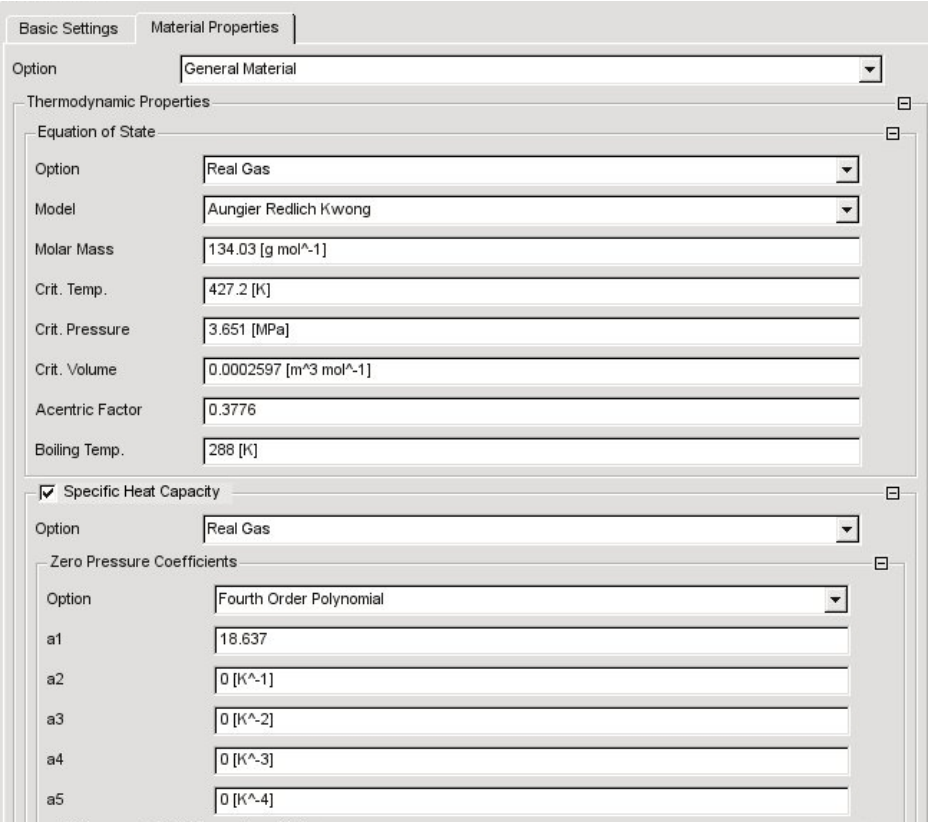

Figure 3.6: Real gas Material Properties in ANSYS CFX-Pre

When selecting the Real Gas option, one of the models offered by ANSYS CFX-Pre has to be chosen. The different models implemented for the solver are:

- Standard Redlich Kwong
- Aungier Redlich Kwong
- Soave Redlich Kwong
- Peng Robinson

According to [18], the Redlich-Kwong equation of state is considered one of the most accurate two-parameter corresponding states equations of state. Aungier modified it in 1995 so that it provides much better accuracy near the critical point. The Peng Robinson and Soave Redlich Kwong equations of state were developed to overcome the limitations of the Redlich-Kwong equations to accurately predict liquid properties and vapour-liquid equilibrium.

Since R-245fa will have a gas state in the process and the expansion properties are close to the critical point, the model chosen is the Aungier Redlich Kwong.

Redlich Kwong models use following cubic equation of state:

$$p = \frac{RT}{v - b + c} - \frac{a(T)}{v(v + b)} \tag{3-1}$$

Where the different parameters depend on the gas constant and critical properties:

$$a(T) = a_0 \left(\frac{T}{T_c}\right)^{-n} \tag{3-2}$$

$$a_0 = \frac{0.42747 \cdot R^2 \cdot T_c^2}{p_c} \tag{3-3}$$

$$b = \frac{0.08664 \cdot R \cdot T_c}{p_c} \tag{3-4}$$

The non-zero parameter c which is added in the standard Aungier version to improve the behaviour of isotherms near the critical point.

$$c = \frac{R \cdot T_c}{p_c + \frac{a_0}{v_c \cdot (v_c + b)}} + b - v_c \tag{3-5}$$

The parameter n depends on the acentric factor of the pure substance. Aungier presented values in [14] for twelve experimental data sets to which he provided a best fit polynomial for the temperature exponent n in terms of the acentric factor, ω.

$$n = 0.4986 + 1.1735 \cdot \omega + 0.4754 \cdot \omega^2 \tag{3-6}$$

And the last thing to specify is the Fourth Order Polynomial coefficients for the heat capacity at constant pressure of R-245fa. The zero pressure polynomial is expressed as

$$\frac{C_p}{R} = a_1 + a_2 \cdot T + a_3 T^2 + a_4 T^3 + a_5 T^4 \tag{3-7}$$

As investigated in Chapter 2 , the desired C_p value is 1156 J kg^{-1} K^{-1} and R is 62.025 J kg^{-1} K^{-1}, the coefficient values will be set to 18.637. The rest of the zero pressure parameters are set to zero.

3.2. Results from the simulations, comparison to the 1-D results and discussion

Pressure values, the numerical results from the simulations calculated at the different areas of the turbine will be calculated using the function "massFlowAve". Like [20] announces, "massFlowAve" gives a mass flow weighted average of the variable. Pressure values will be averaged by the "areaAve" function, which works as "massFlowAve" but giving an area weights average. The area average of a scalar is calculated using equation (3-8) by integrating the scalar times the area divided by the total area over the region. A mass averaged quantity is obtained using (3-9) by integrating the scalar time mass flow divided by total mass flow over the region.

$$areaAve = \frac{\int \varphi \ dA}{A} \tag{3-8}$$

$$massFlowAve = \frac{\int \varphi \ d\dot{m}}{\dot{m}} \tag{3-9}$$

With an area average, the spatially dominant quantity will have the greatest influence on the result. A mass average is more difficult to conceptualize. Mass averaging will return the quantity which is dominant in the flow. When calculating pressure values, conservation has to be taken into account. Area averaging pressure results in summing the forces and dividing by the total area, area averaged pressure is the same as total force over total area. On the other hand, a flow quantity such as Total Pressure or Enthalpy is not spatially conserved. If an average of these is needed, the best option is "massFlowAve".

When regarding variable distributions on surfaces, unless it is otherwise indicated, the surface will be created with the "Turbo Surface" tool with a constant span of 0.5.

As read in [20], the constant span option allows to create a surface at a fractional span value between the hub and the shroud.

3.2.1. Stator inlet

Previously in this chapter, the need of proving the sameness of total and static states at inlet was commented. Before exposing all other results from the simulations, it has to be verified that the inlet boundary conditions given for the simulations lead to the desired static state.

Static and total states share the same entropy but have different enthalpy. The enthalpy difference depends on absolute velocity as it can be proved using (1-1).

In Chapter 2, expected values of absolute velocity and total-static enthalpy difference for both simulations where calculated. Table 3.2 exposes those expectations and shows a comparison between them and the results from the simulations.

	Simulation values	1D Expected values	error [%]
$c_0\ [m/s]$	23.62	24.87	5.3
$h_{t0} - h_0\ [J\ kg^{-1}\ K^{-1}]$	286.2	309.26	8.1

Table 3.2: Expected absolute velocity and total-static enthalpy errors for the ideal gas simulation

The error is calculated with reference to the simulation values as:

$$error = \frac{|1D\ Expected\ value - Simulation\ value|}{1D\ Expected\ value} \cdot 100$$

Shown by the values in Table 3.2, expected values do not differ much from the resulting ones. The low absolute velocity values lead to small total-static deviations.

	Simulation values	1D Expected values	error [%]
$c_0\ [m/s]$	20	20.64	3.2
$h_{t0} - h_0\ [J\ kg^{-1}\ K^{-1}]$	197.9	213.05	7.8

Table 3.3: Expected absolute velocity and total-static enthalpy errors for the real gas simulation

For the real gas simulation, as Table 3.3 evidences, the static-total deviation was well expected and has an even lower value than the ideal gas simulation one.

The fact, that the deviations are so low, indicates parity between the static and the total state values that can be observed in Table 3.4.

	Desired static state	Ideal gas simulation	error [%]	Real gas simulation	error [%]
$p_0\ [MPa]$	0.85	0.84	1.2	0.84	1.2
$T_0\ [K]$	358.15	358.4	0.1	357.9	0.1

Table 3.4: Inlet total-static state deviation for the ideal gas simulation

The errors shown in Table 3.4 are calculated as:

$$error = \frac{|Desired\ static\ state\ value - Simulation\ value|}{Simulation\ value} \cdot 100$$

For the ideal gas simulation, errors committed when assuming equability of total and static states at inlet are low enough to consider it a correct assumption. Hence, it has been demonstrated that the used inlet boundary conditions leads to the desired inlet static state.

3.2.2. Stator

In Chapter 2 it was explained how the main deviations between ideal- and real gas simulations come from the density difference at stator inlet. Figure 3.7 presents the density variation for both simulations at the mentioned turbo surface.

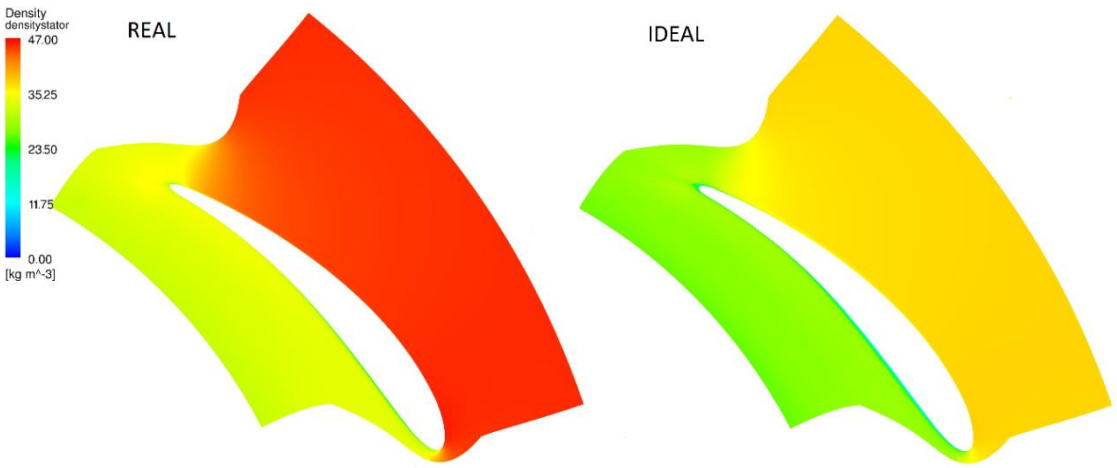

Figure 3.7: Densities through the stator for both simulations

An important deviation in density can be observed. For the ideal gas simulation, the density is always lower than for the real gas one. A decrease in density can be observed in the same region for both simulations. It takes place where the area is reduced by the inlet guide vanes. Because of the area drop, the velocity rises and it causes a density descent.

	Ideal gas simulation	Real gas simulation	Ratio $\left(\frac{\rho_{ideal}}{\rho_{real}}\right)$
Stator inlet density ρ_0 [kg/m^3]	37.75	45.43	0.83
Rotor inlet density ρ_1 [kg/m^3]	24.78	30.09	0.82

Table 3.5: Density values at stator and rotor entries

The results from the simulation are given in Table 3.5. ANSYS results can be compared to the expected results of Chapter 2 in Table 2.6. The density values at stator inlet are like expected in Table 2.6. Densities at stator inlet differ in the compressibility factor at stator inlet, 0.83.

The ratio between ideal and real densities remains, constant through the stator. Taking into account the continuity equation (1-9), the meridional velocities will also show the same ratio, but inversed and the velocity triangles will show the important differences expected in Chapter 2.

3.2.3. Velocity triangles at rotor inlet

The errors calculated in the following tables of this chapter are calculated as:

$$error = \frac{|Real\ gas\ simulation\ value - Ideal\ gas\ simulation\ value|}{Real\ gas\ simulation\ value} \cdot 100$$

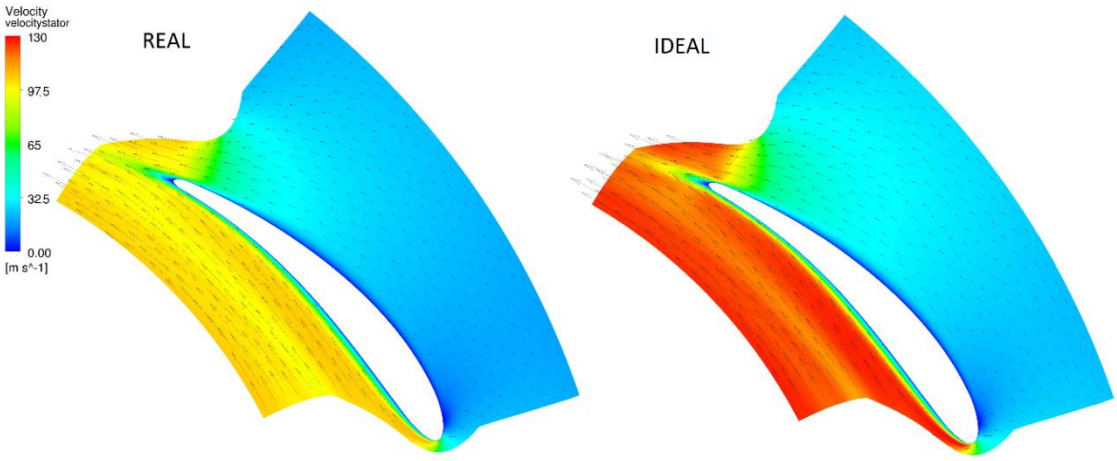

Figure 3.8: Absolute velocities through the stator for both simulations

It is important to have a visual idea of the velocities evolution through the stator regarding Figure 3.8. A significant velocity deviation is shown in Figure 3.8. Ideal gas achieves higher velocities than real gas. A closer look comparing Figure 3.8 and Figure 3.7 reveals the relation between density and velocity that the continuity equation manifests. Namely, a density variation results in a velocity variation. For this reason velocity changes in Figure 3.8 occur exactly where the densities in Figure 3.7 do.

In order to obtain the velocity triangles, the different velocity components can be calculated at "S1R1 Side 2" boundary, which is the rotor inlet.

	Ideal gas simulation	Real gas simulation	error [%]
u_1 [m/s]	130.896	130.896	-
c_1 [m/s]	97.6	81.26	20.1
w_1 [m/s]	48.6442	59.1042	17.7

Table 3.6: "massFlowAve" velocities at rotor inlet

Table 3.6 shows the velocity components from the simulation at rotor inlet. Knowing these three velocity values, the velocity triangle is fixed and the other triangle components can be calculated and seen in Table 3.7.

	Ideal gas simulation	Real gas simulation	error [%]
c_{m1} [m/s]	30.24	24.97	21.1
c_{u1} [m/s]	92.79	77.33	20
α_1 [°]	71.95	72.1	0.2
β_1 [°]	51.57	65	20.7
$\frac{C_{u1}}{U_1}$	0.71	0.59	20.3

Table 3.7: Velocity components at rotor inlet

The ratio calculated with the results from the simulation between real and ideal gas densities leads, thanks to continuity equation, to an equal but inverse ratio between real and ideal meridional velocities.

$$\frac{\rho_{1,ideal}}{\rho_{1,real}} = 0.82 = \frac{c_{m1,real}}{c_{m1,ideal}} \tag{3-10}$$

This relationship between meridional velocities is like expected by the results in Chapter 2. The resulting velocities, though, have lower values than presumed, as it can be observed in Table 2.8.

The issue appears regarding the incidence factor, $\frac{C_{u1}}{U_1}$. The optimum value of 0.85 based on [11] design criteria is not achieved. The ideal gas simulation appears to have an incidence factor of 0.71. It brings to a non-optimal entry in the rotor and this fact will have an important effect on enthalpy change and consequently on efficiency.

As it can be seen, comparing expected values from Table 2.8 with the obtained results from Table 3.6 and Table 3.7, the only precise assumption was guessing the inlet angle α_1. Having the same angle α_1, a decrease in absolute velocity leads to an increase in relative velocity.

The problem is not that the ideal gas simulation shows an incidence factor of 0.71. The issue is that the real gas simulation presents a very different value of 0.59. It means that the flow enters the rotor with a bigger relative angle β_1. Relative angle results from Table 3.7, compared to the optimum value 25.87°, are much higher and suggest a possible inadequate flow through the rotor that should also be analysed.

3.2.4. Flow through the rotor

Figure 3.9 ilustrates the ideal relative streamline flow at rotor inlet.

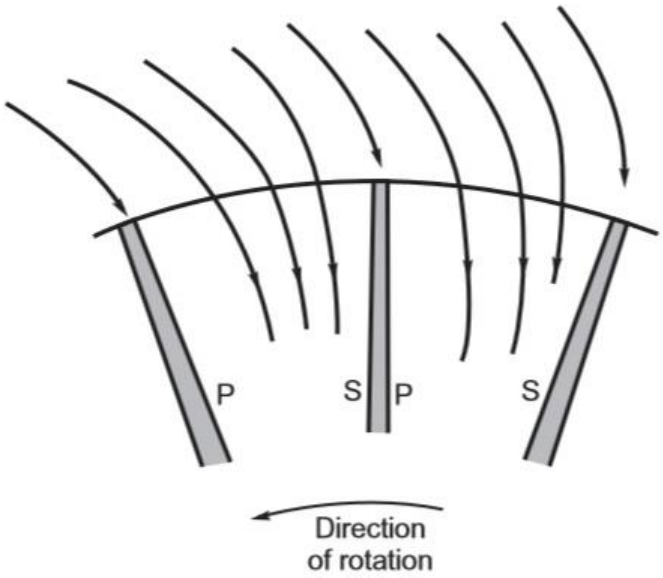

Figure 3.9: Streamline flow at rotor inlet taken from [21]

The static pressure gradient across the passage causes a streamline shift of the flow towards the suction face. As read in [21], stream-function analyses of this flow condition show that the streamline pattern properly locates the inlet stagnation point on the vane leading edge so that the streamline is approximately radial. It is reasoned that only at that flow condition will the fluid move smoothly into the rotor passage.

The relative angles calculated for the simulations, seen in Table 3.7, are too high to suggest an optimum flow through the rotor.

For the ideal gas simulation, the relative streamlines can be plotted on the turbo surface, as it can be observed in Figure 3.10.

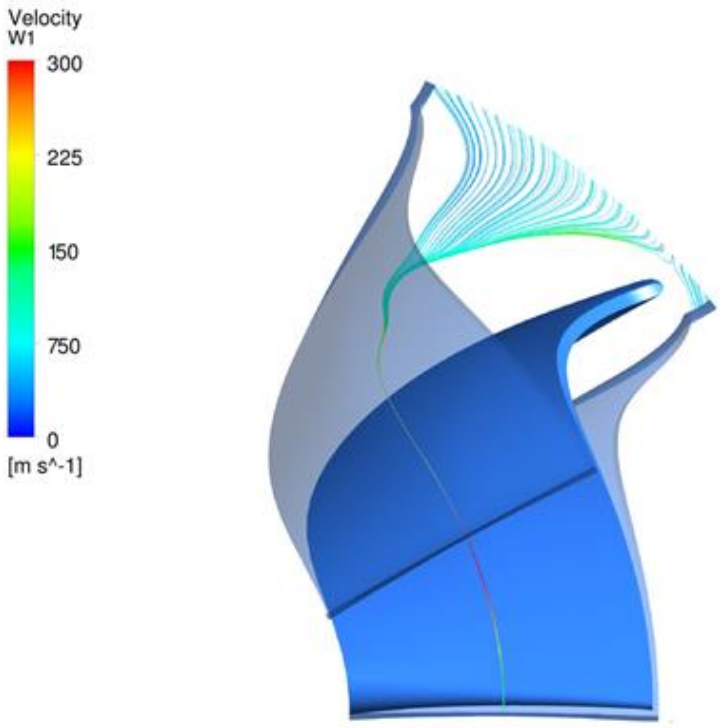

Figure 3.10: Relative streamlines through the rotor for the ideal gas simulation

The streamlines of Figure 3.10 present a radial entrance in the rotor. The stagnation point can be seen at the vane leading edge, which according to Dixon, [21], is recommendable for radial turbines. The more obtuse relative angle of the real gas simulation at rotor entry can lead to more losses through the rotor. For this simulation, the same procedure can be followed to plot the relative flow through the rotor for the real gas simulation.

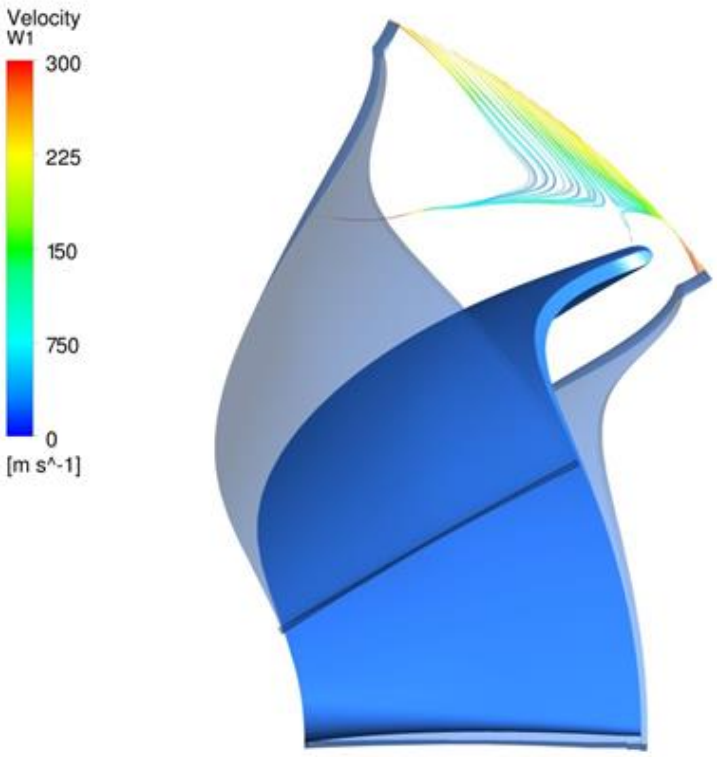

Figure 3.11: Relative streamlines through the rotor for the ideal gas simulation

Figure 3.11 evidence an important deviation from optimum flow conditions. As is can be seen and as it was shown in Table 3.7, the relative flow comes at a higher relative velocity and a too obtuse relative angle. This fact situates the stagnation point on the suction face of the blade, not at its leading edge, and the fluid does not have a smooth flowing through the rotor. It suggests losses that will be verified when analysing the enthalpy change in the rotor.

3.2.5. Outlet state and velocity triangles

After all the commented deviations between ideal- and real- gas simulations, a view on outlet properties will be another good indicative of the discrepancies between the two models.

A comparison of both outlet state values can be seen in Table 3.8.

	Ideal gas simulation	Real gas simulation	error [%]
$p_2[MPa]$	0.4	0.43	6.98
$T_2[°C]$	341.451	349.211	2.22
$\rho_2\ [kg/m^3]$	18.87	21.82	13.52

Table 3.8: Comparison of both outlet states

The deviation between temperatures does not seem to be very significant. The issue comes, though, when regarding variation values: If the temperature variation $T_0 - T_2$ for both simulations is compared, an error of 86.81 % is committed. This fact is of extreme importance, since the enthalpy change for an ideal gas expansion is calculated using equation (2-15).

It is interesting to see if the velocity at outlet is axial and its value in order to know if the total state has to be considered when calculating the efficiency of the cycle. The outlet velocity triangle components for both simulations are shown in Table 3.9.

	Ideal gas simulation	Real gas simulation	error [%]
u_2 [m/s]	75.82	79.13	4.2
c_2 [m/s]	44.16	45.06	2
w_2 [m/s]	40.21	42.05	4.4
c_{m2} [m/s]	18.48	18.19	1.6
c_{u2} [m/s]	40.11	41.22	2.7
α_2 [°]	65.26	66.18	1.4
β_2 [°]	62.64	64.36	2.7

Table 3.9: Outlet velocity triangle components for both simulations

Like stated in [23], the absolute flow at rotor exit should be axial for a nominal design and the meridional velocity c_{m2} should be kept small in order to minimise the exhaust energy loss, unless an exhaust diffuser is fitted to the turbine, which is not the case.

There is no big difference between both outlet absolute velocities. The important conclusion that can be taken here, therefore, is that the outlet absolute velocity is not axial and therefore its value is higher than at a nominal expected design. This situation suggests that the outlet total state will differ from the static one.

3.2.6. Enthalpy change and expansion efficiency

All commented deviations inflict enthalpy variations that cause enthalpy differences between both simulations.

	Ideal gas simulation	Real gas simulation	error [%]
$h_0 - h_1$ $[J\,kg^{-1}\,K^{-1}]$	4603.2	3325.5	38.41
$h_1 - h_2$ $[J\,kg^{-1}\,K^{-1}]$	1446	380.6	279.93
$h_0 - h_2$ $[J\,kg^{-1}\,K^{-1}]$	6049.2	3706.1	63.22

Table 3.10: Enthalpy variations for both simulations.

Table 3.10 exhibits enthalpy changes for both processes. Enthalpy variation results sum up all commented differences between both simulations.

The enthalpy variation through the stator is the one that presents a lower error value and represents a 38 %, which is not acceptable. Its minor value is due, as already discussed, to the lower density value at stator inlet. The ratio between real- and ideal gas simulation densities remains constant through the rotor and due to continuity, at rotor inlet the ideal- and ideal absolute velocities have the same ratio as densities but inversed. Absolute velocity at rotor inlet is directly proportional to the enthalpy variation through the stator, and that is the reason for the enthalpy change deviation through the rotor.

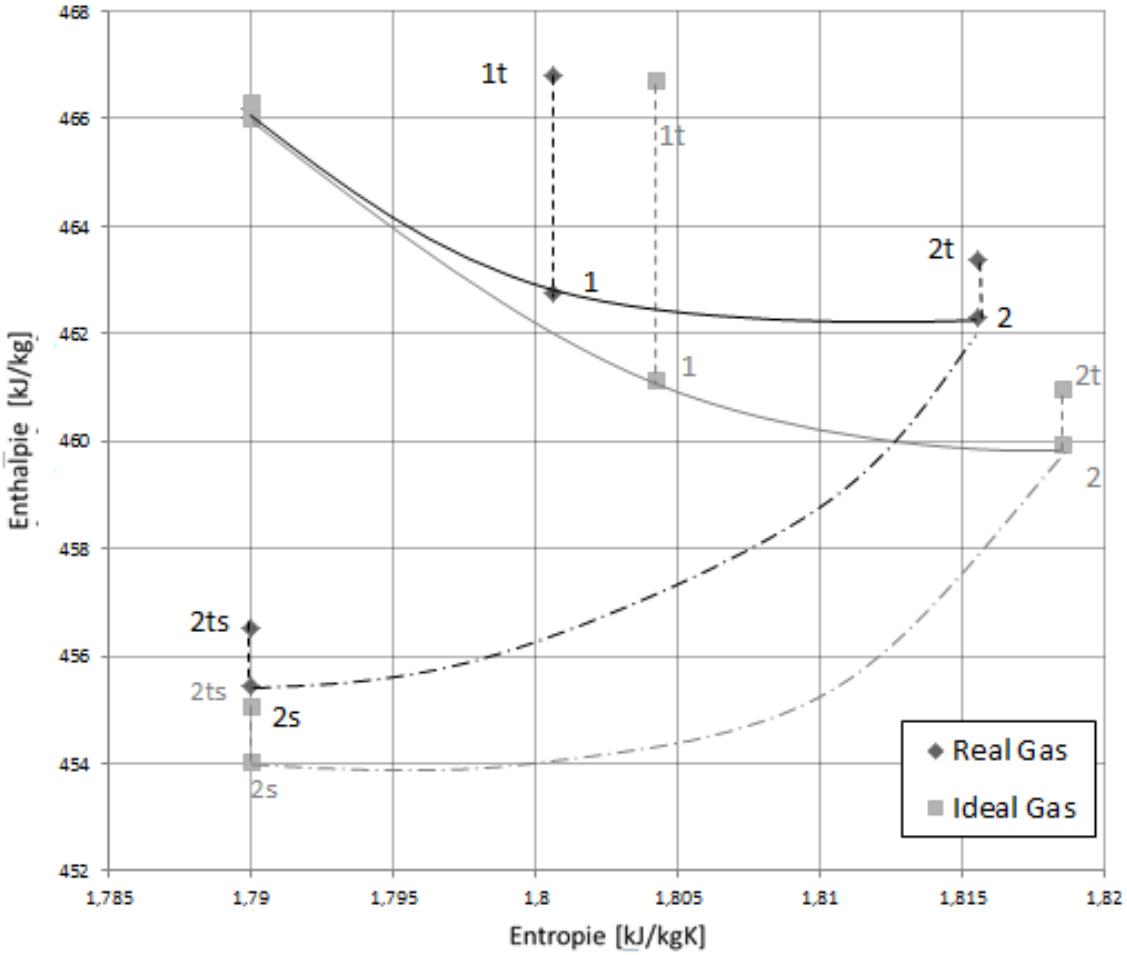

Figure 3.12: h-s diagram

As it can be seen in Figure 3.11, the relative streamlines of the real gas simulation do not have a radial entry. This fact causes high losses that have an effect on the enthalpy variation as observed in Table 3.10.

Both enthalpy variation errors bring to an enthalpy variation error through the whole process of 63.22 %, which indicates the huge difference between bot gas models. Before comparing efficiencies, it has to be taken into account, that the two simulations do not have the same outlet ideal state. The reason for this difference is that the two simulations show different outlet preassures. This issue and the differences in enthalpy and entropy between both simulations can be observed in Figure 3.12.

	Ideal gas simulation	Real gas simulation	error [%]
$h_0 - h_{2s}\ [J\ kg^{-1}\ K^{-1}]$	15000	14000	7.14
$h_{0t} - h_{2s}\ [J\ kg^{-1}\ K^{-1}]$	15286.2	14197.9	7.67
$h_0 - h_2\ [J\ kg^{-1}\ K^{-1}]$	6049.2	3706.1	63.22
$h_{0t} - h_{2t}\ [J\ kg^{-1}\ K^{-1}]$	5296.5	2626.3	98.36
$\eta_{ts} = \frac{h_0 - h_2}{h_0 - h_{2s}}$	0.4	0.26	53.85
$\eta_{ts} = \frac{h_{0t} - h_{2t}}{h_{0t} - h_{2s}}$	0.35	0.18	94.44

Table 3.11: Enthalpy variation and efficiency comparison

Two important conclusions can be drawn from the results of Table 3.11.

Because of the outlet absolute velocity, which is not axial and has a higher value than at the nominal design, the difference between total and static enthalpy is also higher than it should be and the total enthalpies have to be taken into account when calculating the total to static efficiency. As it can be seen, total to static efficiency calculated with total enthalpies is lower than the same calculated without taking static efficiency into account.

The other conclusion has to do with the big difference between both simulation efficiencies. If the velocity triangles where like expected for a nominal design, the gap between the efficiencies would not be so large, but the thing is: All deviations previously explained in Chapter 3 lead to a big deviation between enthalpy variations in the process and to the conclusion that the ideal gas model does not match with the real gas one.

3.3. Summary

The main results are:

- At stator entry, both simulations are set to have the same temperature and pressure. Ideal gas and real gas differ at this point in their density. In fact, the ratio between ideal and real densities at stator entry is the compressibility factor.
- The ratio between real and ideal densities remains constant through the stator. Both simulations use the same turbine and the same mass flow, which remains constant through the process. That is the reason why, due to continuity, a change in density entails a proportional change in meridional absolute velocity.
- Having the same stator, the two simulations own the same inlet absolute angle α_1. Owning the same inlet absolute angle, the proportion between ideal and real meridional velocities at rotor entry will remain for ideal and real absolute velocities. The stator enthalpy change is equal to $\frac{1}{2}c_1^2$, and the proportion between absolute velocities has an even more significant effect on real/ideal stator enthalpy change variation.
- The dissimilarity between real- and ideal gas absolute velocities at rotor inlet leads to a change in their velocity triangles geometry. These changes imply disparities in relative flow through the rotor. Different relative flows through the rotor result in different enthalpy variations through it.

All commented deviations between ideal- and real- gas simulations cause different states at the end of the expansion, which already means an important variance. Enthalpy change deviations imply a contrast between the efficiencies resulting from both simulations that is the final indicator of the disparity between both models. The real gas model is thus the valid model and will be utilized for the optimization of the turbine.

Chapter 4: Study on turbines with different inlet width for an ORC process with an electrical work output of 3.5 kW

In this part of the project the turbine simulated in Chapter 3 will be optimized in order to reach an electrical power output of 3.5 kW. The first optimizing process is based on the turbine inlet width and the turbine will be simulated for three different widths. The second part concerns the optimization process. The rotational velocity of the rotor will be changed to adapt the velocity triangles at rotor inlet in order to achieve an optimal entry in the rotor.

4.1. Aim of the study and expansion properties

The results from the realized simulations carried out up to this point revealed that with the considered boundary conditions and using the real gas model, the turbine cannot reach a pressure of 0.35 MPa. The aim of the simulations performed in Chapter 4 is to optimize the threated turbine in order to reach an output power of 3.5 kW. The main optimization process is the change of the turbine inlet width value. Following conditions imposed by the application of the turbine have to be fulfilled:

- The evaporator of the cycle works at a pressure of 0.85 MPa and the condenser operates at a pressure of 0.35 MPa. Since these pressure values cannot vary, the pressure conditions are unyielding.
- The mass flow through the cycle is 0.215 kg/s. Higher values of mass flow would entail an adaption of the stator.

4.2. Turbine geometries

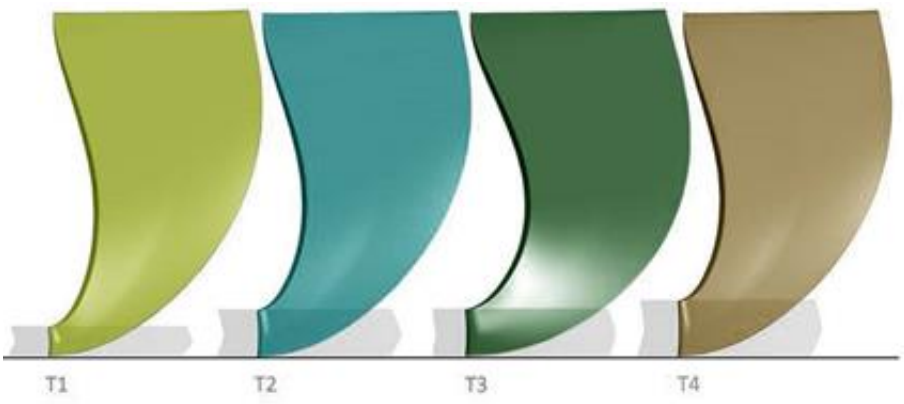

Figure 4.1: Comparison of blade widths

The dimensions of the turbines are shown in Table 4.1 . The prior difference between the four turbines investigated in this part of the project is their inlet width, as it can be seen in Figure 4.1. Turbine 3 is the turbine for which the effects of Ideal Gas assumption were investigated. The blades of the turbines 2 and 3 have the same inlet width. The difference between them is the orientation of the blades at inlet as it can be seen in Figure 4.2. With the exception of Turbine 3, all other turbines have a radial blade orientation at rotor inlet.

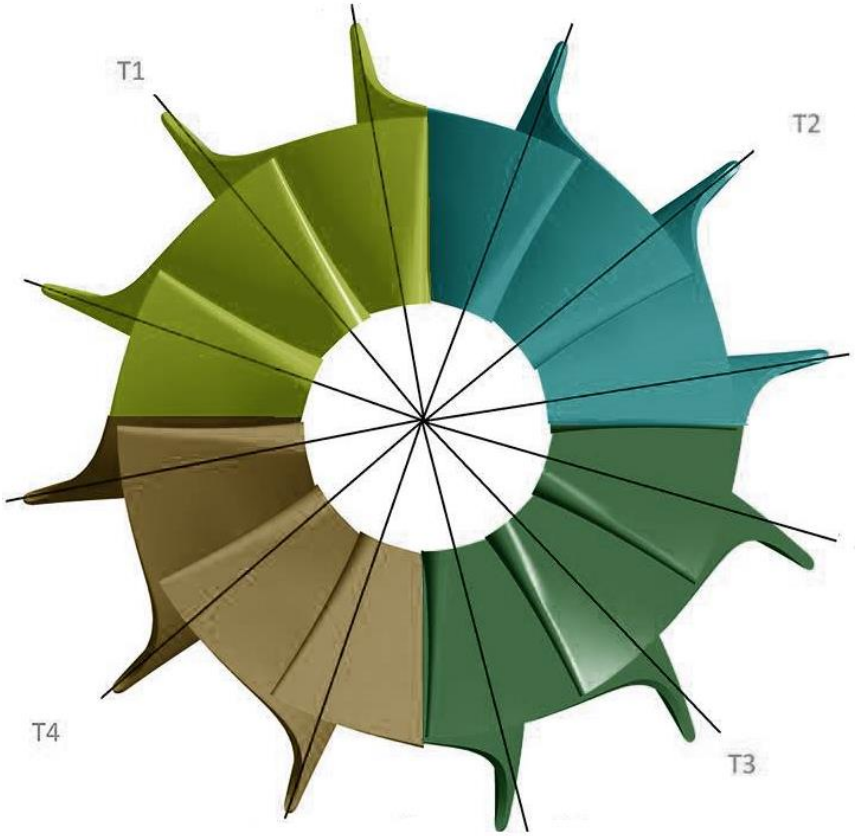

Figure 4.2: Comparison of the blade orientation

In order to study the influence of the inlet width, all other geometric properties have to be the same for the different turbines, so that the effects shown in the results are only due to the width variation. Turbines 2 and 3 seem to have the same measures; the difference between both turbines is the orientation of the blade at rotor inlet.

[mm]	T1	T2	T3	T4
D_1		48		
b_1	1.7	2.7	2.7	3.2
r_{2s}		18.2		
r_{2h}		7.2		
Blade orientation at rotor inlet	Radial	Radial	Bent	Radial

Table 4.1: Blade dimensions for all turbines

4.3. Simulation properties

The most detailed part in this chapter is the utilization of ANSYS Turbogrid software in order to create the geometry of the turbines and their mesh. The ANSYS CFX-Pre process is very similar to the one threated in Chapter 3 and their variances will be properly described in in this chapter 4.

4.3.1. Obtaining turbine geometry and mesh with ANSYS TurboGrid

All turbines share the same stator geometries but with a varying width. The ITSM provided the curves for one stator and they had to be adapted to the different widths of the four rotors. The meshing process was carried out considering the 6 steps that [16] suggests and all four turbines follow the same procedure.

1. Define the geometry:

The stator and the rotor will be meshed separately. In order to define the geometry the user provides the three curves, indicates the number of Bladesets and the principal axis of rotation, which will be the z-Axis. The stator consists of eleven blades and the rotor possesses twelve blades. Once the geometry is defined, the topology can be created. For the rotor a shroud tip of a 0.1 mm normal distance is produced.

2. Define the topology object.

The topology, as [16] exposes, is a structure of blocks that acts as a framework for positioning the mesh elements. Topology blocks represent sections of the mesh that contain a regular pattern of hexahedral elements. It is invariant from hub to shroud, which are the 2-D layers where the topology will be edited.

For the topologies of rotor and stator and its blades, the ATM Optimized method is chosen. It automatically computes a default mesh and sets the base mesh dimensions. Each unique mesh dimension has an edge refinement factor that is multiplied by the base mesh dimension and a global size factor to determine the final size of the mesh dimension. Local mesh size adjustments can be made by adjusting the local edge refinement factors. The overall mesh size can be changed by editing the Mesh Data object.

3. Optionally modify the Mesh Data object to adjust the number of nodes.

The selected method is the Target Passage Mesh Size, since this option enables the user to choose the approximate mesh size (in nodes), and lets ANSYS TurboGrid compute the mesh dimensions automatically, including the size factor. For the rotor, between “coarse”, “medium” and “fine” option, as well as for the stator, a “fine” node count is designated. It will generate approximately 250,000 nodes.

Once the topology is constructed, the 3D Mesh can be generated.

4. Generate the 3D Mesh and optionally investigate the mesh and refine as necessary.

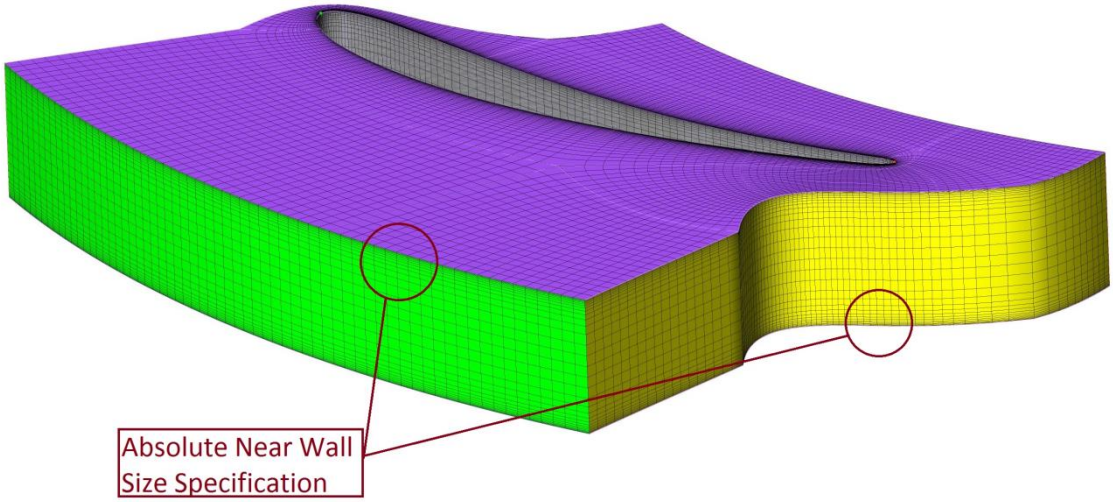

Figure 4.3: Stator ATM Optimized mesh

All the commented Topology and Mesh Data options result in the mesh in Figure 4.3. The refinement of the mesh consists on the increased number of elements next to the hub and the shroud. The “absolute” Near Wall Element Size Specification method allows the user to directly set the near wall spacing directly and is therefore used for the calculations.

Rotor mesh is illustrated in Figure 4.4. As it has a tip between the blade and the shroud, the rotor mesh requires more refinement.

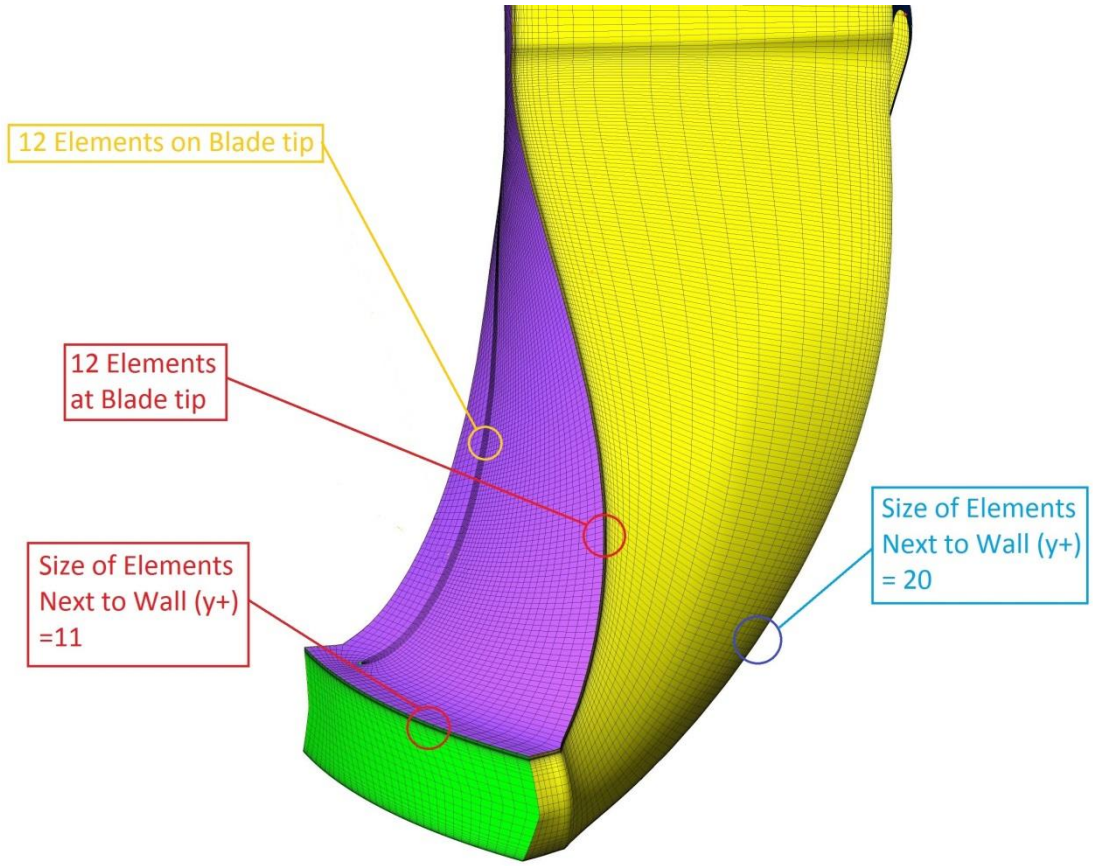

Figure 4.4: Rotor ATM Optimized mesh

The nominated Near Wall Size Specification for the rotor is the Y Plus Method. This option lets the user specify the approximate maximum y+ height for the blade. ANSYS TurboGrid uses commented information to compute the Edge Refinement Factor. The specified offset and the actual offset may differ. Not all the elements near the surface of the blade will have a constant height, but they will generally be at or less than the specified maximum. Furthermore, the y+ calculation is only approximate. 12 Elements of size 11 will be used in order to refine the shroud tip. For the passage, 20 elements near the hub will be generated. Finally, for the blade the number of elements on the shroud tip is set to 12; the refinement can be observed in the yellow circle, where there are a greater number of elements for the shroud tip.

	Total Nodes	Total Elements
Stator T1, T2, T3, T4	256742	241140
Rotor T1	471712	385188
Rotor T2	423640	392413
Rotor T3	422170	389548
Rotor T4	422606	390748

Table 4.2: Mesh Statistics

As a result of the meshing process, Table 4.2 shows the number of nodes and elements created for each turbine Rotor and Stator. As it can be seen, all Stators have approximately the same number of nodes

5. Save the mesh to a file.

The last step is to save the rotor and the stator mesh.

4.3.2. Pre-processing with ANSYS CFX-Pre

The pre-processing of the simulations for this part of the project has a lot of parities with the Pre-processing of the first part of the thesis. In fact, the domains and interfaces do not change. For a comfortable understanding, the names of the domains and interfaces will not be changed.

The results from Chapter 3 showed up the big difference between the real gas model and the ideal gas one. The ideal gas model is not a good approximation for the pressure region of the ORC-Process expansion. For that reason, the material model used for these simulations is the real gas one. Exactly the same model as the real gas one explained in Chapter 3.

The difference between both Pre-processes lays on the boundary conditions, as it can be seen in Table 4.3. In the past simulations no outlet pressure was given as boundary condition and the mass flow through the turbine was set to 0.215 kg/s. For the calculations of this chapter no mass flow is fixed as boundary condition. Instead of this condition, an outlet pressure of 0.35 MPa is imposed.

Boundary condition	Past simulation	Present simulations
$T_{t0}\ [K]$	358.15	358.15
$p_{t0}\ [MPa]$	0.85	0.85
$p_2\ [MPa]$	-	0.35
$\dot{m}\ [kg/s]$	0.215	-
$\omega\ [rpm]$	50000	50000,48000,46000

Table 4.3: Comparison of the past and present simulations

The reason for the commented change is that, as seen in Chapter 3, the turbine does not reach a pressure of 0.35 MPa with the given mass flow. The pressure condition at outlet given by the working characteristics of the condenser is immovable, since it can only work at this pressure. It is possible for turbine to adapt to the mass flow by changing the absolute inflow angle of the stator by moving its guided vanes.

Another important novelty of the present simulations is the rotational speed. Three different rotational speeds will be tested for these simulations: 50000, 48000 and 46000 rpm. The reason for the change of rotational speed is to adapt the velocity triangles at rotor inlet.

4.4. Results from the 50000 rpm calculation

Firstly in Chapter 4, the simulations for the rotational speed of 50000 rpm will be exposed and discussed. For these simulations, the focus of the study will be the inlet width variation. After that, the optimization varying the rotational speed value will be investigated by revealing and commenting the simulations for the other rotational speeds.

4.4.1. Specific speed and total-to-static efficiency

Rohlik analytically investigated in [17] the performance of 90° inward-flow radial turbines in order to determine optimum design geometry for various applications as characterised by specific speed. His method was used to determine the design point losses and corresponding efficiencies for various combinations of nozzle exit flow angle, rotor diameter ratio and rotor blade entry height to exit diameter ratio.

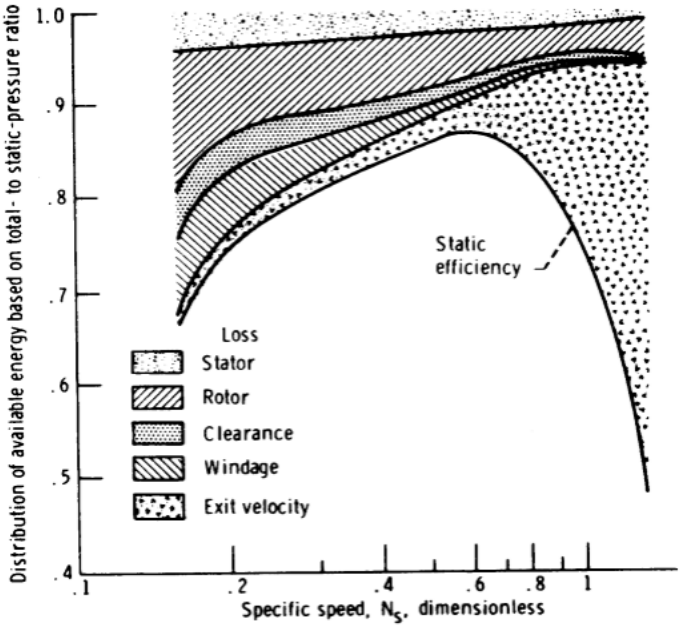

Figure 4.5: Distribution of losses along envelope of maximum total-to-static efficiency from [17]

The distribution of losses for optimum geometry over specific speed range can be seen in Figure 4.5. Loss distributions change as a result of the changing ratio of flow to specific work .

To situate the case on the Rohlik diagram specific speed should be calculated. As explained in [21], specific speed depends on the rotational speed w, the volumetric flow rate Q_2 at rotor exit and the total-to-total enthalpy drop Δh_{0s}.

$$n_s = \frac{N Q_2^{0.5}}{\left(\Delta h_{t,s}\right)^{0.75}} \tag{4-1}$$

The point is to understand which parameter changes when the width of the blade at rotor inlet is varied. The rotor inlet diameter is the same for all four turbines. The rotational velocity at rotor inlet is also the same for all of them since all the four rotors spin at 50000 rpm. The total to static enthalpy change is calculated as:

$$\Delta h_{t,s} = h_{0,t} - h_{2,s} \tag{4-2}$$

The inlet operating point for all simulations is identical, because this state is fixed with total pressure and total temperature as a boundary condition. The outlet isentropic enthalpy has the same entropy as the inlet state and depends on the outlet pressure. Since the outlet pressure is a boundary condition all turbines will have approximately the same total to static enthalpy. The volume flow rate can also be expressed as a function of mass flow rate and density:

$$Q_2 = \frac{\dot{m}}{\rho_2} \tag{4-3}$$

The parameters that change by changing the rotational speed are the mass flow and the total density at turbine outlet. It is important to take every effect into account:
In order to know the possibly total density deviation between the four turbines, the p-h diagram is helpful. The total state at turbine outlet is supposed to be very close to the static state by considering the outlet absolute velocity low enough. If it is true, the density variation between them should not be high, because the density lines in the diagram are fairly horizontal. Total density at outlet will have little change when varying rotor inlet width.

The mass flow, though, is directly related to the inlet width by the continuity equation (1-9) and if inlet velocity does not change much, a modification of the rotor inlet width will affect the mass flow in a proportional way.

	Turbine 1	Turbine 2	Turbine 3	Turbine 4
$b_1[mm]$	1.7	2.7	2.7	3.2
$\dot{m}$ [kg/s]	0.142	0.233	0.233	0.279
$\frac{\dot{m}}{b_1}$	0.84	0.86	0.86	0.85

Table 4.4: Relationship between inlet width and mass flow

The values in Table 4.4 show how inlet width and mass flow are related by the continuity equation. The third row values confirm the direct dependence of mass flow on the inlet width. The fact that all turbines have a similar value indicates that the inlet velocities will be also very analogous. Already demonstrated how inlet width has an effect on the mass flow through the turbine, its influence on specific speed can be analysed.

	Turbine 1	Turbine 2	Turbine 3	Turbine 4
$b_1\ [mm]$	1.7	2.7	2.7	3.2
$\dot{m}$ **[kg/s]**	0.142	0.233	0.233	0.279
$\rho_{t,2}$	18.422	18.861	18.663	18.923
n_s	0.34	0.44	0.43	0.48

Table 4.5: Comparison between rotor inlet and specific speed

Specific speed values rise due to the inlet width increase, as it is shown in Table 4.5. Another conclusion that can be taken with the results from the simulations is the less change in outlet total density. According to Figure 4.5 the losses for Turbine 1, which has a lower specific speed value, will be the highest of all turbines. Turbine 2 and 3 will have similar losses and Turbine 4 is supposed to present inferior losses. Less loss means more efficiency, and Rohlik tendency can be observed in Figure 4.6 within the range of specific speed. Turbine 2 and 3 have the same efficiency and Turbine 1 has the lowest value.

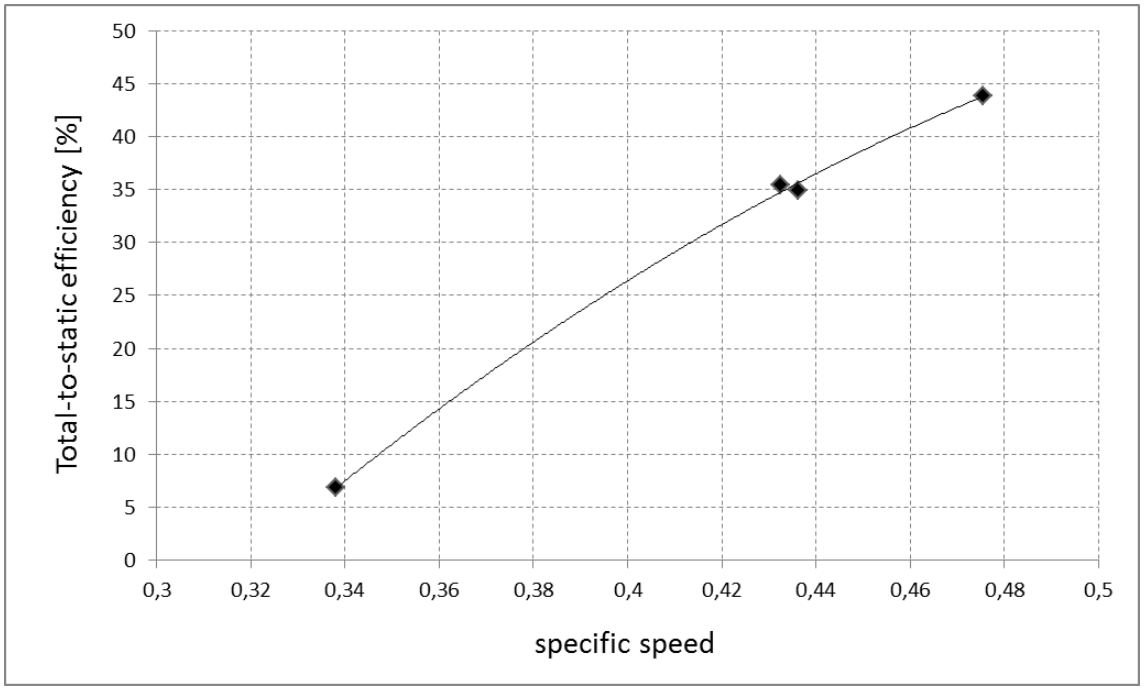

Figure 4.6: Total to static efficiency for the simulations at 50000 rpm

In fact, Turbine 1 efficiency value is the lowest one. For this reason, it is necessary to investigate the flow through the rotor presented in Figure 4.7. The relative velocity streamlines clearly show a reverse flow region in the rotor.

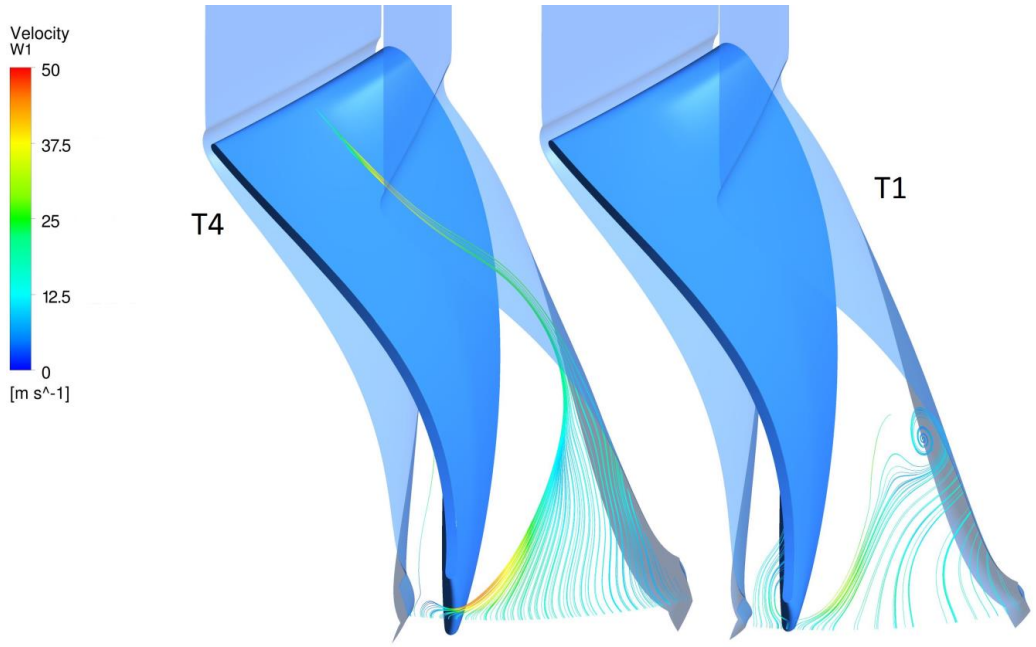

Figure 4.7: Relative flow on a 0.5 constant span Turbosurface in ANSYS CFX-Post for turbines 1 and 4

The dysfunction observed in the relative flow through the rotor is the reason for the low efficiency. This leads to an analysis of the velocity triangles at rotor entry.

4.4.2. Velocity triangles at rotor inlet

Variables	Turbine 1	Turbine 2	Turbine 3	Turbine 4
u_1 [m/s]	130.9			
c_1 [m/s]	97.8	105.99	104.34	108.08
w_1 [m/s]	45.57	41.6	42.05	38.95
α_1 [°]	72.63	73.74	73.96	74.75
β_1 [°]	52.14	44.48	46.73	43.12
$\lambda = -\frac{C_{u1}}{U_1} + \frac{u_2}{u_1}\frac{c_{u2}}{u_1}$	-0.51	-0.59	-0.6	-0.62
$\frac{C_{u1}}{U_1}$	0.71	0.78	0.77	0.8

Table 4.6: Velocity triangles components at rotor inlet

Three important remarks should be commented after investigating Table 4.6. The first one is the pronounced difference that exists between Turbine 1 and the other turbines. The problem is the low value of absolute velocity of Turbine 1. All turbines share the same absolute angle, since all of them have the same stator. They share also the same rotational velocity. Because of that, the lower value of absolute velocity has a direct effect on the relative velocity and its angle. The relative angle is more obtuse for Turbine 1 and its relative velocity is higher. The velocity triangle alterations lead to a value for the incidence factor, $\frac{C_{u1}}{U_1}$, of 0.71 when according to [11] it should be nearby 0.85.

A second remark is that a comparison between Turbines 2 and 3 seems to be interesting, since the importance of the blade orientation at rotor inlet can be investigated. Changing the inlet orientation of the blades has an immediate influence on the relative angle β_1. This variation, though, is not significant, since all other velocity components for Turbines 2 and 3 are very analogous. A look at Figure 4.8 helps to see the effect of varying the orientation of the blade. As it can be read in [17], stream-function flow analyses of the flow condition show that the streamline pattern properly locates the inlet stagnation point when there is an "optimum" angle β_1. The flow at the stagnation point is approximately radial. The radial position of the stagnation point helps avoiding the flow from separating from the suction surface near the leading edge. The stagnation point of Turbine 2 is less radial than the one of Turbine 3. It does not lead to important losses in this case, since Turbine 2 shows a total-to-static efficiency of 34.88% and Turbine 3 a 35.44%.

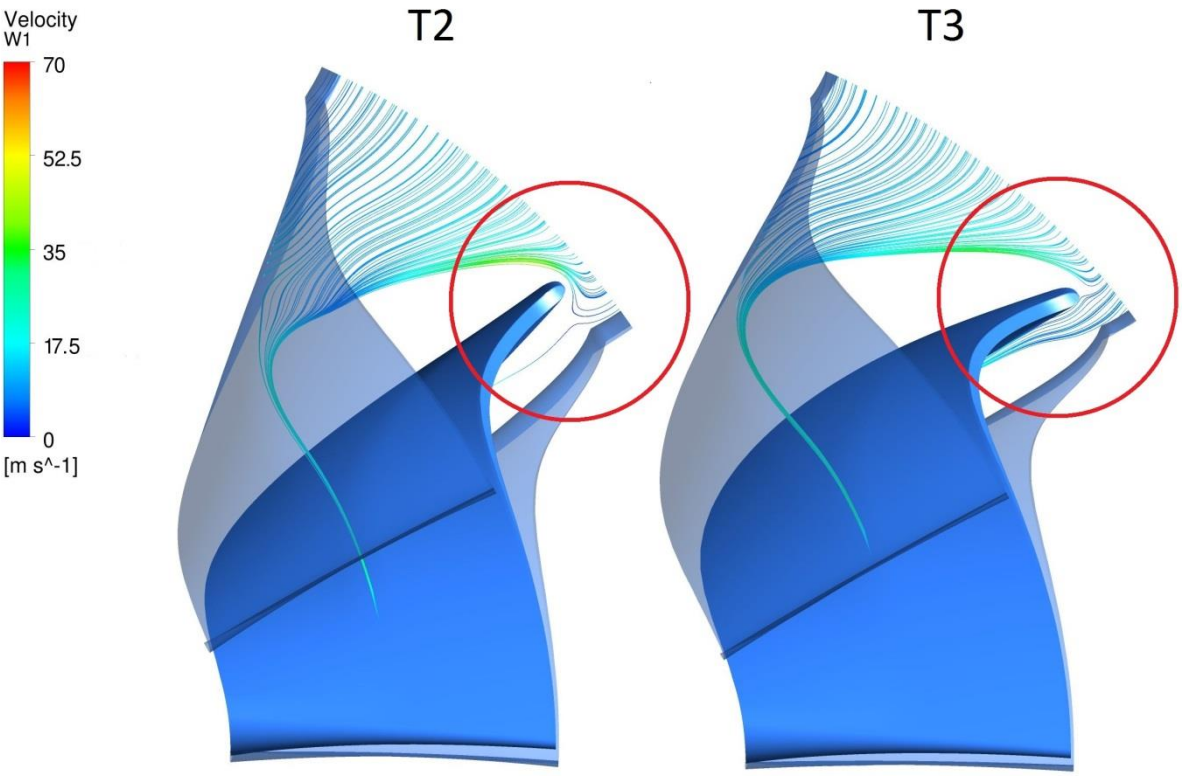

Figure 4.8: Rotor inlet relative streamlines for Turbines 2 and 3

The third fact to point out from Table 4.6 has to do with the relation between C_{u1} and U_1. Considering the optimal value of 0.85 commented in [11], all turbines seem to differ much from this value. A change in rotational speed will change the velocity triangles at rotor inlet and will lead this relation closer to the optimum value.

4.4.3. Output power

The rotor inlet velocity triangles of the turbines require an optimization, but before carrying it out, it is essential to take a look at the output power that the different turbines produce and proof if 3.5 kW are already supplied. The specific work done by the fluid on the rotor is

$$\Delta W = h_{0,t} - h_{2,t} \cong h_{1,t} - h_{2,t} \tag{4-4}$$

Therefore, the power subtracted from the fluid is:

$$P = \left(h_{0,t} - h_{2,t}\right)\dot{m} \tag{4-5}$$

Not taking into account the losses of the generator, the electrical power supplied by each turbine can be seen in Figure 4.9, none of the turbines at 50000 rpm reach the desired electrical output power of 3.5 kW. The turbine that more power output delivers is Turbine 4. The reasons for this higher work output of Turbine 4 are its higher efficiency and mass flow. An optimization process has to be carried out in order to increase the power output of the turbines.

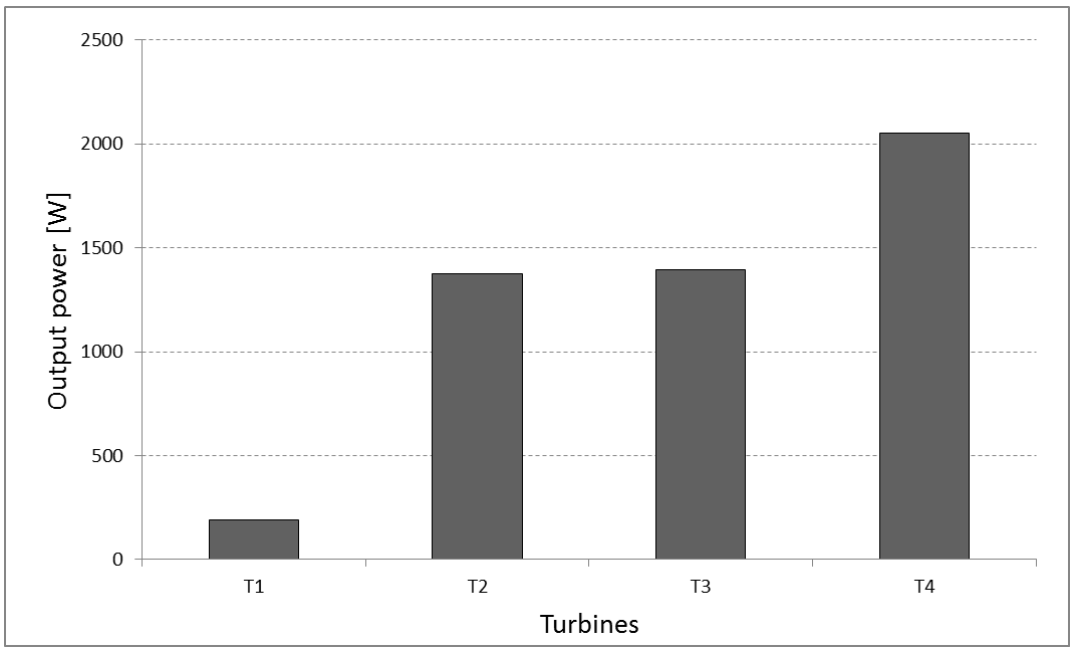

Figure 4.9: Output electrical power

4.5. Results from the optimization process calculations

Since the geometries of the rotors and stators of this work were given by ITSM and are not modified within this work, the only way of altering the velocity triangles at rotor entry is to vary the rotational speed. It is possible, by varying the rotational speed, to achieve an optimal geometry of the velocity triangles at rotor entry. The objective of the optimization process is therefore to achieve values of $\frac{C_{u1}}{U_1}$ close to 0.85.

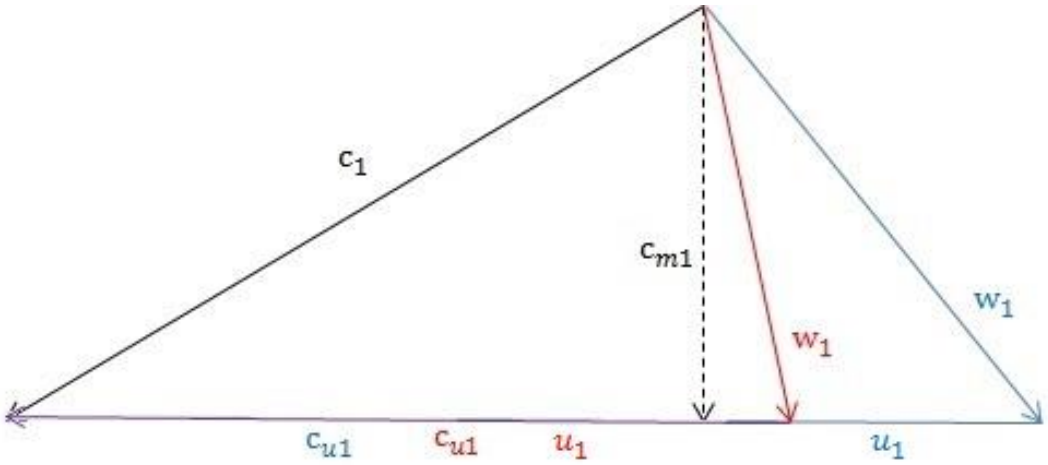

Figure 4.10: Velocity triangle change expected after the optimization process

The velocity triangle modification can be observed in Figure 4.10. The blue lines symbolize the velocity triangle for 50000 rpm and the blue one the velocity triangle for a lower rotational speed. If the rotational speed is reduced, the absolute velocity value and its direction should not vary since the stator remains the same. When reducing the rotational speed, c_{u1} remains constant and that is the reason why the incidence factor will be increased.

An issue appears when considering the effects on the specific speed. Specific speed is directly proportional to rotational speed, as appreciated in its definition (3-1) found in [21], and although the volumetric flow rate did not change much, rotational speed will have a lower value for minor rotational speeds. It can be observed in Figure 4.5 how the losses increase when decreasing the specific speed, but a minor specific speed does not imply a lower efficiency in general. In this case, for example, it has been demonstrated that the specific speed will decrease when reducing the rotational speed. Nevertheless it also provides a better rotor entry incidence that will reduce the losses through the rotor, which are the most significant for low values of specific speed.

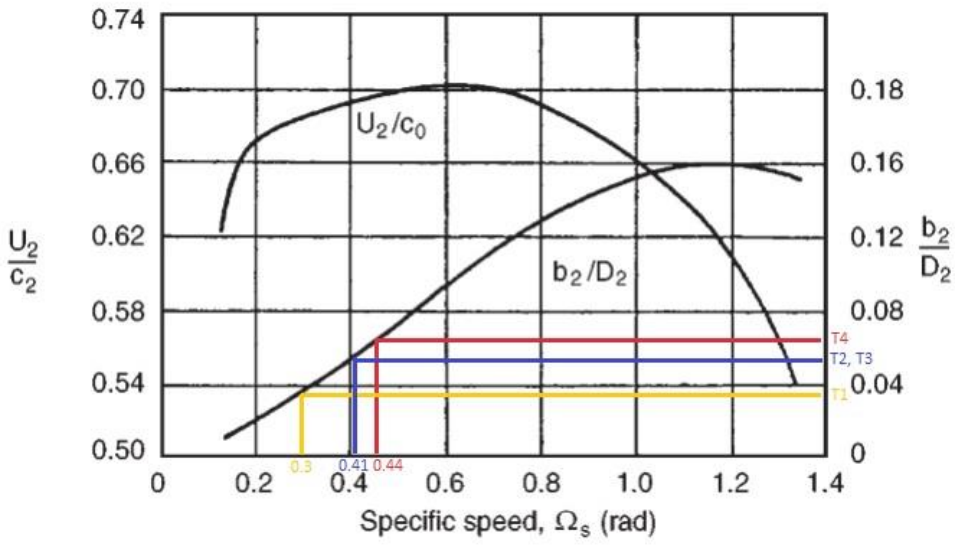

Figure 4.11: Variation in nozzle blade height/rotor inlet diameter corresponding to maximum total-to-static efficiency with specific speed

Another way of justifying the use of lower rotational speeds is presented in Figure 4.11, found in [23]. Figure 4.11 presents the specific speed that should be accomplished for each of the inlet heights in order to achieve the maximum total-to-static efficiency. The values of specific speed for the different turbines rotating at 50000 rpm, shown in Figure 4.11, are all above the optimum values corresponding to Figure 4.11. It corroborates the validity of the optimization process. The rotational speed will be lowered in two steps to 48000 rpm and 46000 rpm.

The first thing which should be analysed is the evolution of the incidence factor $\frac{C_{u1}}{U_1}$ and the velocity triangles to see if the changes are like expected. After that, it has to be verified if the incidence factors are closer to their optimal values seen in Figure 4.11. Once known that their specific speeds are close to these optimal values, the new efficiencies and power outputs can be found out in order to evaluate the improvement resulting from the optimization.

4.5.1. Incidence factor

The incidence factor for all turbines, shown in Figure 4.12, grows when lowering the rotational speed. All turbines, except Turbine 1, achieve and/or exceed the optimum value of 0.85. Turbine 1 needs lower rotational velocities in order to reach the optimum value, but the efficiencies shown by it, due to the reverse flow in its rotor passage dissuade from optimizing it.

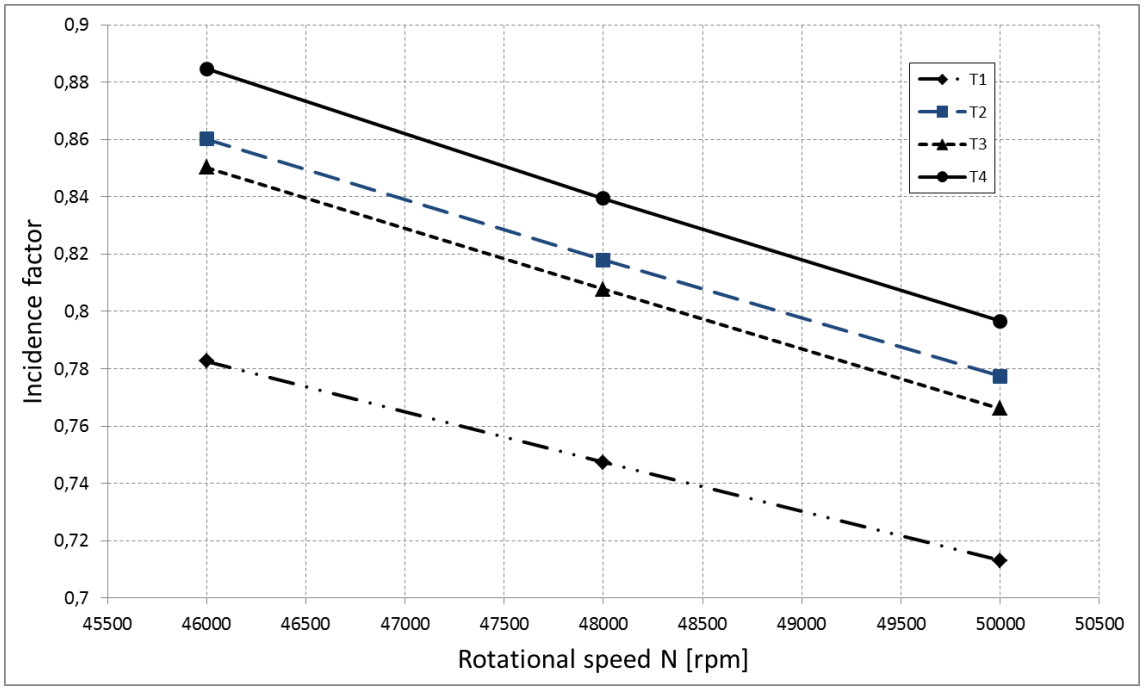

Figure 4.12: Incidence factor for the different inlet widths and rotational speeds

The effects of changing the rotational speed on the incidence factor are satisfactory. The velocity triangles provide a better entry in the rotor and therefore a better total-to-static efficiency and a higher power output.

4.5.2. Specific speed

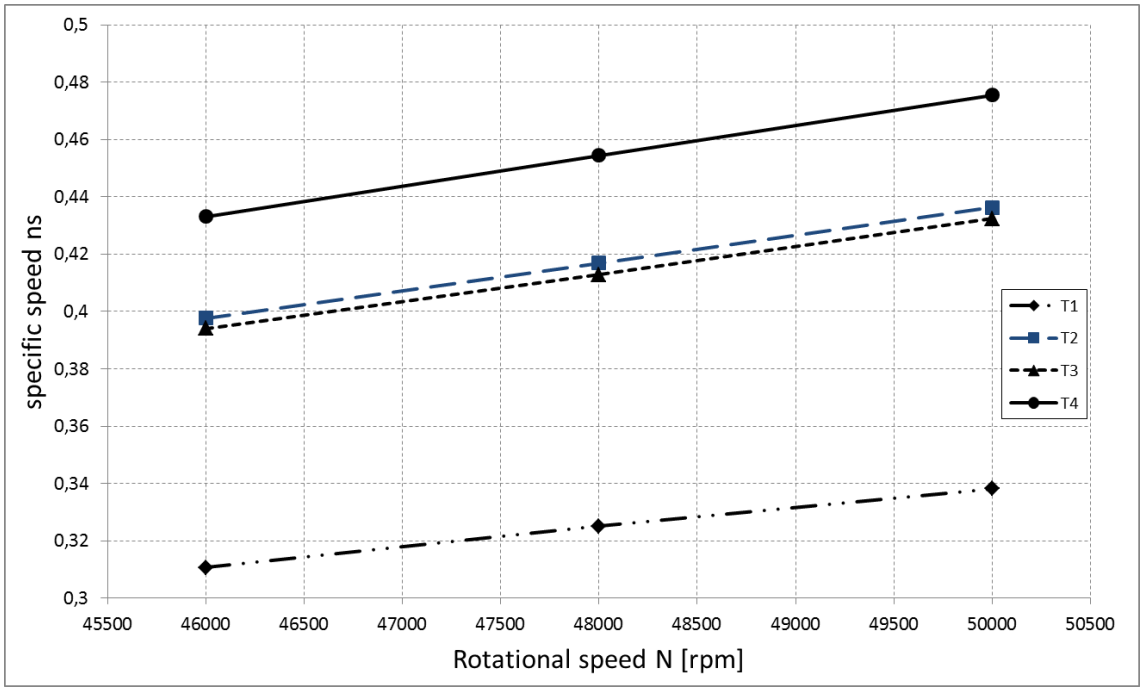

Figure 4.13: Specific speed for the different inlet widths and rotational speeds

Specific speed values resulting from the calculations can be observed in Figure 4.13. As predicted, the specific speed values fall when reducing the rotational speed. To evaluate the validity of the values shown in Figure 4.13 they can be compared to the optimal values considered by Rohlik in [23]. Turbine 1 practically reaches the design value of 0.3. Turbines 2 and 3 have a specific speed value nearby the design value, 0.41. Turbine 4 specific speed value is also close to the design one.

In fact, all turbines show a specific speed close to the optimal by the rotational speed of 46000 rpm according to Figure 4.11. For this reason, the efficiencies of all turbines are expected to have their highest values for the simulations at the rotational speed of 46000 rpm.

4.5.3. Total-to-static efficiency

The commented tendency can be observed in Figure 3.14. For all turbines, the highest value of total-to-static efficiency was expected for the rotational speed of 46000 rpm.

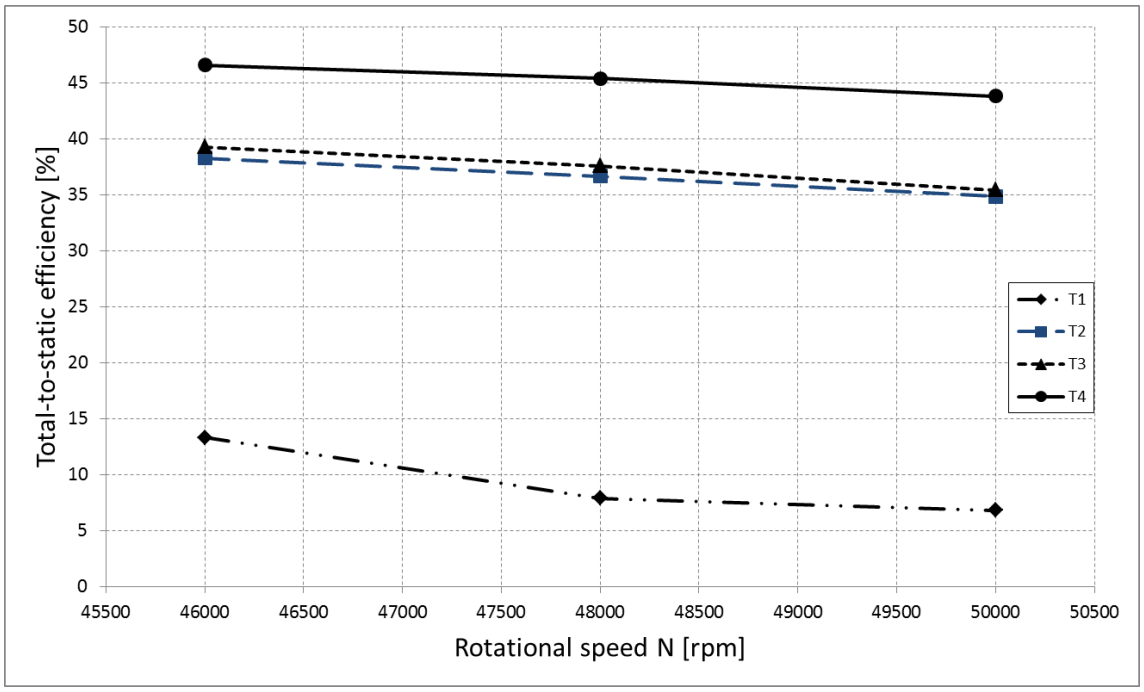

Figure 4.14: Total-to-static efficiency for the different inlet widths and rotational speeds

Three remarks can be taken regarding Figure 4.14:

- Although experiencing an improvement, Turbine 1 still has low values of total-to-static efficiency. The reason for this are the reverse flow that still appear in the rotor passage at the rotational speed of 46000 rpm.
- Turbine 2 and 3 efficiency values do not differ much for any of the rotational speeds. It seems that the change in the orientation of the blade at rotor inlet does not lead to higher efficiencies.
- Turbine 4 reaches the highest total-to-static efficiency of all the turbines at all rotational speeds.

Table 4.7 sums up the improvement carried out for all turbines. As shown, Turbine 1 presents the more significant improvement.

Total-to-static efficiency [%]	50000 rpm	46000 rpm	Improvement [%]
Turbine 1	6.85	13.34	94.74
Turbine 2	34.88	38.28	9.75
Turbine 3	35.44	39.29	10.86
Turbine 4	43.83	46.6	6.32

Table 4.7: Efficiency improvement

4.5.4. Electrical power output

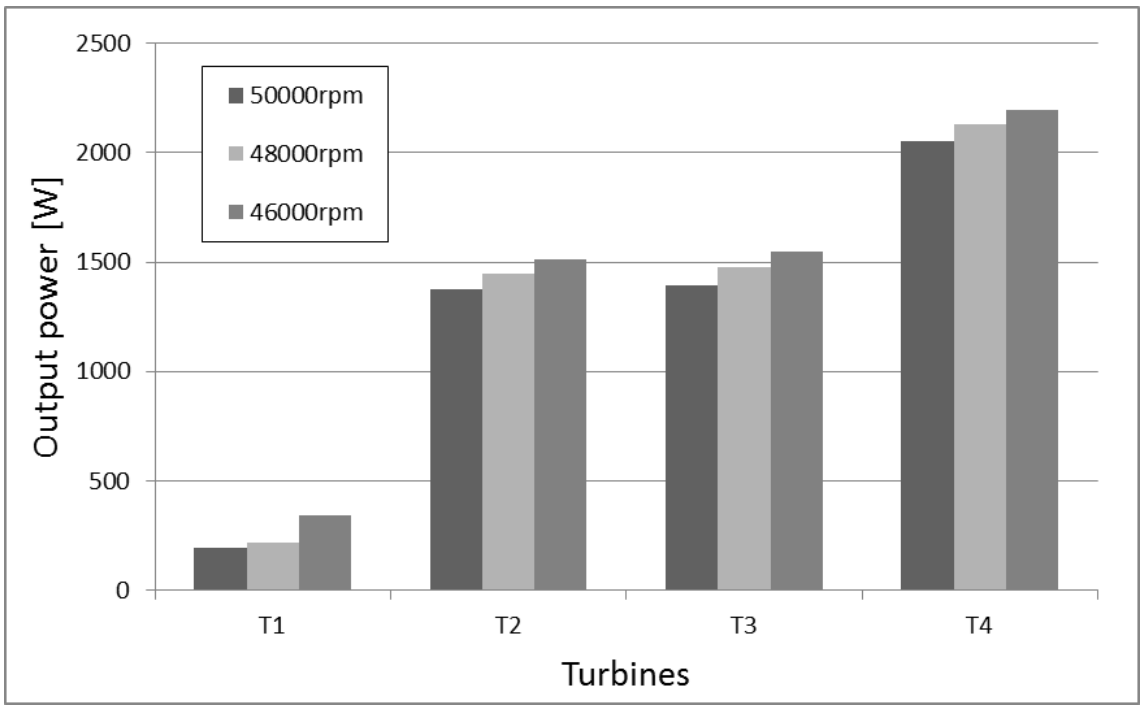

Figure 4.15: Output power for the different inlet widths and rotational speeds

As the isentropic state at outlet does not change, the power outputs at a rotational speed of 46000 rpm exhibit similar values of improvement to the values achieved by total-to-static efficiency. The results for output power can be observed in Figure 4.15. The growth of the output power is based on the efficiency betterment. The improvements are calculated as:

$$improvement = \frac{|50000\ rpm\ value - 46000\ rpm\ value|}{50000\ rpm\ value} \cdot 100$$

Output power [W]	50000 rpm	46000 rpm	Improvement [%]
Turbine 1	191.88	345.31	79.96
Turbine 2	1374.92	1513.97	10.11
Turbine 3	1395.63	1549.31	11.01
Turbine 4	2052.21	2193.55	6.89

Table 4.8: Output power improvement

The turbine that experiences a better improvement is Turbine 1, but its efficiency and output power still differ a lot from the results of all other turbines. The target of the optimization was to reach a total output power of 3.5 kW but as it can be seen in Table 4.8 the highest output power achieved is 2.19 kW.

4.6. Summary

In this chapter the optimization process of the radial turbine investigated in the previous chapter is exposed. The aim of the optimization is to reach an output of 3.5 kW. The first optimization process is based on the inlet width of the turbine. Therefore three more turbines are simulated. Turbine 1 has a shorter width and Turbine 4 has a higher width. Turbine 2 has the same width as Turbine 3 but the same blade orientation as Turbines 1 and 4, so that the three different widths can be compared. A greater width value means a higher specific speed value and fewer losses according to Rohlik diagram. The results are satisfying and indicate a higher efficiency and a greater power output for the turbine with a greater width than Turbine 3. Anyway, none of the turbines reach an output power of 3.5 kW. This issue suggest a further optimization.

The second optimization process is based on the rotational velocity of the rotor. The reason for the rotational speed variation is to adapt the rotor inlet velocity triangles in order to reach an optimal entry in the rotor. All turbines improve their velocity triangles at rotor inlet and their total-to-static efficiency at lower values of rotational speed. Turbine 4 reaches the better efficiency and the highest output power but it is less than 2.5 kW.

Chapter 5: Conclusions

The vast challenge of modelling R-245fa and optimizing a radial turbine resulted in some useful conclusions. These ideas, which are presented separately, can inspire the reader convinced of going one step further to try other ways of modelling R-245fa and other ways of optimizing the turbine.

For this reason, the last sections of this thesis will first summarize the important points to have in mind, observed during the realization of the thesis, when modelling the fluid and optimizing the turbine. It will finish with some advice for the way forward to an additional optimization process.

5.1. Real/Ideal Gas assumption effects

The ideal gas laws describe only an idealized behaviour of the fluid, which the real gas can only approach under certain conditions. These conditions are low pressures or very high temperatures. Regarding its p-h diagram, the area where the refrigerant R-245fa follows the ideal gas law can be easily recognized where the isothermal lines fall vertical. The inlet pressures for the expansion of an Organic Rankine Cycle are located where the isothermal lines bend instead of being vertical. The effects of modelling R-245fa with the ideal gas model in ANSYS CFX for a given expansion of an ORC cycle have been investigated by comparing the results using an ideal gas model and a real gas one.

The inlet state values of the ideal gas model differ from the inlet state values of the real gas model. This difference causes unalike state values and velocity components at rotor inlet. One of the most important design foundations is the rotor inlet velocity triangles. The results show that the incidence factor at rotor entry differs. That means that if the turbine is designed for an ideal gas, when using a real gas the rotor entry will diverge from the expected one. The dissimilarity between both models leads to a difference in total-to-static efficiency of 94.44%.

The conclusion for the first part of the thesis is clear: The ideal gas model is not valid for the ORC expansion. The real gas model set up for the refrigerant R-245fa provides plausible results and can be utilized for the simulations of the second part of the project.

5.2. Optimization

The first optimization process is based on the effects of different inlet widths in order to supply an electrical power output of 3.5 kW. The original turbine inlet width is 2.7 mm and two other widths are investigated in the second part of the project: 1.7 mm and 3.2 mm. The use of different widths can be justified with the resulting specific speeds. Specific speed is extensively used to describe turbomachinery operating requirements. Low specific speeds mean higher losses. When augmenting the inlet width, the specific speed increases and leads to fewer losses and higher efficiencies.

The results of the first optimization process are satisfying. The efficiency of the turbine is enhanced in a 25.71% by the turbine with the bigger width. This improvement is very significant, but the electrical power output that the turbine provides is 2 kW and is still below 3.5 kW. Another important result concerns the mass flow. The turbine needs a mass flow of 0.279 kg/s, which is superior to the one flowing through the original turbine, 0.215 kg/s. It indicates the need of changing the stator vanes geometry or its angle in order to modify the mass flow.

The unreached output power suggests another optimization process. Since the stator and the rotor geometries were given and are not changed in the project, the only way of optimizing the process is to change the rotational speed of the rotor. The incidence factors at rotor entry resulting from the first optimization process are all below the optimum value. A decrease in rotational speed is considered to adapt the velocity triangles and raise the incidence factors to their optimal value.

The results of the second optimization process confirm the hypothesis done. All turbines ameliorate their incidence factor to their optimal value. This fact upgrades all total-to-static efficiencies. The turbine with the 3.2 mm width presents the lowest efficiency amelioration, 6.89% but the highest power output. This is, though, lower than 2.2 kW, which still stands underneath the desired value of 3.5 kW.

5.3. Recommendations for further work

The reader interested in validating the real gas model performed in the thesis should try to simulate R-245fa in a different way. As already commented in the project, there are three ways of modelling a gas in ANSYS CFX:

- Ideal gas model
- Real gas model
- Using Real Gas Property (RPG) Tables

It has been demonstrated, that using an ideal gas model for an ORC expansion process leads to wrong results. An innovating idea would be to investigate the use of Real Gas Property Tables. ANSYS CFX uses by this method a number of data tables during the CFD solution. Evaluating fluid properties through a complex equation of state like Aungier Redlich Kwong, the one used in this thesis, could lead to significant computing overhead.

Accessing these tables is much faster than evaluating properties from the equation of state and it could be an important benefit, especially for heavier simulations.

The optimization carried out in the project ameliorates the efficiency of the turbine and enhances this way the output power provided by the turbine. Although having improved these properties of the turbine, the power output does not achieve the desired value of 3.5 kW. The tendency shown suggests the desired output power by greater widths. For that reason a way to carry on the optimization process performed in the thesis could be:

- Investigate higher values of inlet width. Changing the inlet width has shown significant progresses in the efficiency and output power of the turbine. In order to achieve 3.5 kW of output power, greater inlet widths should be simulated.

Another issue that comes off the results from the optimization is that the mass flow through the turbine surpasses the value of 0.215 kg/s , which was the original mass flow. The mass flow that is needed by the turbine with a greater width is 0.279 kg/s. Once found a turbine with the desired output power, its stator should be adapted:

- Study different configurations for the stator guided vanes. That is necessary for the purpose of adapting the mass flow. These changes would also have an effect on the rotor inlet triangles and should also lead to an additional improvement of the turbine efficiency and output power.

The complexity and extension of R-245fa modelling requires joint efforts and the present thesis pretends to have contributed in this joint doing its bit: providing a first real gas model for R-245 fa and testing it by optimizing a turbine. The optimization offers encouraging results and suggests possible ways of carrying on the optimization in order to attain the desired output power.

Bibliography

1. *Simulation and economic analysis of a CPV/thermal system coupled with an organic Rankine cycle for increased power generation.* **Kosmadakis, G.** 2011, Solar Energy, pp. 308-324.

2. *Power production from a Moderate-Temperature Geothermal Resource.* **Brasz, Joost J.** 2005.

3. *Analysis of energetic, design and operational criteria when choosing and .* **J. Facão, A.C. Oliveira.** s.l. : Proceedings of the ASME 2009 International .

4. *On the systematic design and selection of optimal working fluids for Organic Rankine Cycles.* **Papadopoulos, AI (Papadopoulos, Athanasios I.), Stijepovic, M (Stijepovic, Mirko) and Linke, P (Linke, Patrick).** Thessaloniki (Greece) : Applied Thermal Engineering, 2010.

5. *An examination of regenerative organic Rankine cycles using dry fluids.* **Mago, Pedro J.** Mississippi : Applied Thermal Engineering, 2008, Vol. 28.

6. *Unconventional working fluids in organic Rankine-cycles for waste energy recovery systems.* **Maizza, V.** 3, s.l. : Applied Thermal Engineering, 2001, Vol. 21.

7. *A study of organic working fluids on system efficiency of an ORC using low-grade energy sources.* **T.C. Hunga, S.K. Wanga.** Taiwan : ELSEVIER, 2010, Vol. 35.

8. *HFC-245fa: An overview of properties and aplications. .* **Soffientini, Cesare.**

9. National Institute of Standarts and Technology. [Online] http://webbook.nist.gov/chemistry/fluid/.

10. **A. Whitfield, N.C. Baines.** *Design of Radial Turbomachines.* s.l. : Longman, 1990.

11. **Michael Casey, D. Phil (Oxon).** *TC_4: Turbines.* Stuttgart : ITSM, 2010/2011.

12. **Glassman, Arthur J.** *Turbine design and application.* Washington, DC : National Aeronautics and Space Administration, 1994.

13. **Moran, Michael J.** *Fundamentals of Engineering Thermodynamics, seventh edition.* s.l. : John Wiley & Sons, 2012.

14. **Baehr, Hans D.** *Thermodynamik: Grundlagen und technische Anwendungen.* s.l. : Springer, 1996.

15. **Stanitz, John D., Ellis, Gaylord O.** *Two-Dimensional Flow on General Surfaces of Revolution in Turbomachines.* s.l. : NATIONAL AERONAUTICS AND SPACE ADMINISTRATION CLEVELAND OH LEWIS RESEARCH CENTER, 1952.

16. **ANSYS.** *ANSYS TurboGrid User's Guide.* 2013.

17. **Rohlik, H. E.** *Analytical determination of radial inflow turbine design geometry for maximum efficiency.* Washington : NASA, 1968.

18. **ANSYS.** *ANSYS CFX- Pre User's Guide.* 2013.

19. *A Fast, Accurate Real Gas Equation of State for Fluid Dynamic Analysis Applications.* **Aungier, R. H.** 1995, Vol. Journal of Fluids Engineering.

20. **ANSYS.** *ANSYS CFD-Post User's Guide.* 2013.

21. **S. L. Dixon, C. A. Hall.** *Fluid Mechanics and Thermodynamics of Turbomachinery seventh edition .* 2013.

22. *Two-equation eddy-viscosity turbulence models for engineering applications.* **Menter, F. R.** s.l. : Aiaa Journal - AIAA J, Vol. 32.

23. **Rohlik, H. E.** *Optimum design geometry for high radial inflow turbine performance efficiency.* Washington : NASA, 1968.